Applied Catalysis B: Environmental 318 (2022) 121803

Contents lists available at ScienceDirect

Applied Catalysis B: Environmental

journal homepage: www.elsevier.com/locate/apcatb

# Activity and *in situ* DRIFT studies on vanadia catalysts during oxidative dehydrogenation of sulfur-contaminated methanol

Niina Koivikko [a], Satu Ojala [a], Tiina Laitinen [a], Felipe Lopes da Silva [a,b,c], Lauri Hautala [b], Zouhair El Assal [a], Mari Honkanen [d], Minnamari Vippola [d], Mika Huuhtanen [a], Marko Huttula [b], Teuvo Maunula [e], Riitta L. Keiski [a,*]

[a] Environmental and Chemical Engineering (ECE), Faculty of Technology, University of Oulu, P.O. Box 4300, FI-90014 Oulu, Finland
[b] Nano and Molecular Systems Research Unit, University of Oulu, P.O. Box 3000, FI-90014 Oulu, Finland
[c] MAX IV Laboratory, Lund University, Box 118, 22100 Lund, Sweden
[d] Tampere Microscopy Center, Tampere University, P.O. Box 692, FI-33014, Finland
[e] Global Catalyst Competence Center, Dinex Finland Oy, 41330, Vihtavuori, Finland

ARTICLE INFO

*Keywords:*
Environmental catalysis
*in situ* DRIFT
*in situ* Raman
AP-XPS
VOC utilization

ABSTRACT

Silica-titania (70/30) supported vanadium catalysts were prepared, characterized, and studied in oxidative dehydrogenation of sulfur-contaminated methanol. The quality of vanadia species is dependent on temperature and gas conditions during preparation, support type, support specific surface area and $VO_x$ surface density. For example, upon heating the amount of $V_2O_5$ decrease along with formation of polymeric species. Such changes may occur also during the catalytic reaction. The reaction experiments and characterization results showed that the stability of polymeric vanadia species and total acidity has a connection with better formaldehyde production performance. The best performance was observed for $N_2$-calcined silica-titania catalyst. Easy reducibility of the catalyst, as in the case of reference catalysts, leads to further oxidation of formaldehyde.

## 1. Introduction

The supported vanadium-based catalysts are known to be efficient in commercial-scale formaldehyde production from methanol, and in environmental applications such as NOx removal and oxidation of chlorinated volatile organic compounds (CVOCs) [1–3]. The earlier studies related to vanadia catalysts have been devoted especially to find the structure-activity relationships through investigating the effects of support type, composition, as well as vanadia surface coverage and quality of species [4–9]. The most used support materials for vanadia are $SiO_2$, $TiO_2$, $Al_2O_3$, and $ZrO_2$. Recently, also $HfO_2$ has been studied. [10–15]

Correct selection of the support material for a catalyst is important since the performance of the whole catalytic system is significantly affected by the properties of the support. Titania ($TiO_2$) is considered as a highly advantageous support for vanadia as the interaction of vanadia with titania is strong [16]. Despite advantageous properties, including chemical stability, of titania, poisoning in the presence of sulfur has been reported [17]. Combination of silica ($SiO_2$) and titania ($TiO_2$) introduces better resistance to sulfur, provides higher mechanical strength, and improves the thermal stability [18–21]. The drawback of silica is the weak interaction with vanadia due to the inert nature of silica. This leads easily to weaker dispersion of the active phase and formation of vanadium pentoxide ($V_2O_5$) crystallites locally. Based on Burcham et al. [22], the density of the active vanadia surface species is similar on most oxide supports at the monolayer coverage, up to where vanadia is present only as tetrahedral $VO_4$ species. After the monolayer coverage is reached, also crystalline $V_2O_5$ species are observed. For titania, the monolayer coverage is achieved with vanadium surface density of ~7.9 V atoms $nm^{-2}$. In contrast to the other metal oxides, the formation of $V_2O_5$ micro crystallites has been detected already below the monolayer coverage in the case of silica support. Gao et al. [23] were able to achieve maximum $VO_4$ coverage on silica with vanadium surface density of 2.6 V atoms $nm^{-2}$ without forming $V_2O_5$ micro crystallites. Crystalline $V_2O_5$, have been reported to have lower activity than the monomeric/polymeric species of vanadia in methanol oxidative dehydrogenation. Gao et al. [23] observed also that vanadia species are isolated on the silica support, which is not typically the case for the other metal oxides.

* Corresponding author.
*E-mail address:* riitta.keiski@oulu.fi (R.L. Keiski).

https://doi.org/10.1016/j.apcatb.2022.121803
Received 17 May 2022; Received in revised form 21 July 2022; Accepted 27 July 2022
Available online 2 August 2022

Nevertheless, using the silica-titania binary oxide support, the advantages of these two support materials could be potentially combined while minimizing the drawbacks of the corresponding single oxide supports.

The most common way to utilize organic emissions is their use in energy production, even other options exist as presented by Ojala et al. [24]. The research reported in this paper arises from the possibility to utilize industrial volatile organic compound emissions in chemicals production, which is a fresh alternative for the emission abatement. The work focuses on formaldehyde production from sulfur-contaminated methanol, which may originate for example from wood pulp production. Vanadia supported on silica-titania binary oxide ($V_2O_5/SiO_2$+$TiO_2$(30%)) has earlier proven to be active in oxidative dehydrogenation of methanol in the presence of methyl mercaptan [13, 14,25]. Still, the material characteristics or their connections with the performance of the catalyst are not fully understood. The single oxide supported vanadia catalysts have been examined earlier in converting (non-contaminated) methanol to formaldehyde for example by the research group of Burcham and Bell [22,26–31]. Furthermore, oxidation of methyl mercaptan as a single reactant has been studied for example by Wachs [32–38]. In this work, the earlier studies [13,14] are extended to investigate a mixture of methanol and mercaptan, mixed oxide support, and how the changes in calcination treatment influence the final catalyst characteristics and the activity.

The calcination atmosphere is known to influence the particle size and thus the dispersion of the active phase on the support. Traditional ways to influence the dispersion are to vary the metal loading and the pore diameter of the support or to use different thermal treatments during the catalyst preparation. [39,40] In this case, also the interaction between vanadia and the support is important, since the V-O-support bond has been earlier postulated to be the most active species in the reaction in concern [41]. The thermal stability of the supported vanadia is known to depend on the support material and the melting point of vanadia. The melting point of $V_2O_5$ ($T_{mp}$) is 690 °C [42]. Increasing the temperature increases the mobility of the atoms, which can be described by empirically defined Tamman (0.5 $T_{mp}$) and Hüttig (0.3 $T_{mp}$) temperatures. [43,44] The values calculated for $V_2O_5$ demonstrate a poor temperature stability of vanadia and forecast mobility of vanadia species already at typical reaction temperatures. Strong vanadia-support interaction, as in the case of $TiO_2$, could potentially improve the thermal stability of the vanadia species. In this study, two supports having high and low $SiO_2$ content were investigated.

The activities of the catalysts were studied in oxidative dehydrogenation of contaminated methanol (MeOH). Methyl mercaptan (MM) was used to represent the sulfur contaminant, since it is often observed in pulp mill emissions [45,46]. The main reaction studied was methanol oxidative dehydrogenation to formaldehyde [1]:

$$CH_3OH + 1/2O_2 \rightarrow CH_2O + H_2O \quad (1)$$

In addition, during the experiments, $CO_2$ can be formed by Reaction 2. Formaldehyde can also react further to $CO_2$ and CO according to Reactions 3 and 4:

$$CH_3OH + 3/2O_2 \rightarrow CO_2 + 2H_2O \quad (2)$$

$$CH_2O + 1/2O_2 \rightarrow CO + H_2O \quad (3)$$

$$CH_2O + O_2 \rightarrow CO_2 + H_2O \quad (4)$$

In the presence of methyl mercaptan, additional formaldehyde formation arises from oxidative desulfurization of methyl mercaptan [45]:

$$CH_3SH + 2O_2 \rightarrow CH_2O + SO_2 + H_2O \quad (5)$$

As a by-product, dimethyl disulphide may appear [45]:

$$2CH_3SH + 1/2O_2 \rightarrow (CH_3)_2S_2 + H_2O \quad (6)$$

The oxidative dehydrogenation of methanol was first studied *in situ* for selected catalysts. Then, reaction experiments were carried out to survey the bulk-activity of the prepared catalysts also in presence of methyl mercaptan. The catalytic materials were thoroughly characterized aiming to explain the phenomena observed.

## 2. Experimental

### 2.1. Material preparation

In this study, two different compositions of support, *i.e.*, $SiO_2$+$TiO_2$(30%) and $TiO_2$+$SiO_2$(5%) were studied. $TiO_2$ represents a reducible support having a strong interaction with vanadia species, while $SiO_2$ is a non-reducible acidic material the main role of which is to increase the sulfur tolerance of the catalyst. The selection of Si-Ti ratio was made based on our earlier result where the Si-Ti ratio of 70:30 was found as the optimal ratio [14]. The Si-Ti ratio of 5:95 was used as a reference, and the material was supplied by a company. A 1.5% vanadia loading was used in the case of the silica-rich support and different calcination treatments were performed to study the influence of calcination on the vanadium species. The high surface area of the $SiO_2$+$TiO_2$(30%) support allows high vanadia dispersion. The reference catalyst had a 3% vanadia loading.

The following chemicals were used in the catalyst preparation: titanium butoxide ($Ti(OBu)_4$, TBOT, 97% Sigma-Aldrich), tetra ethoxy orthosilicate ($Si(OC_2H_5)_4$, TEOS, 98%, Sigma-Aldrich), ethanol A ($C_2H_5OH$, EtOH Merck), nitric acid ($HNO_3$, 65%, Sigma Aldrich), vanadyl acetylacetonate ($VO(acac)_2$, 98%, Sigma-Aldrich), and methanol ($CH_3OH$, 99.9%, Merck). The $SiO_2$+$TiO_2$(30%) support was prepared using the sol-gel method. In the sol-gel method, appropriate amounts of titanium and silicon precursors were first dissolved in absolute ethanol (1:14 EtOH molar ratio). A few drops of nitric acid were added to the solution, and then ultra-pure water ($H_2O$) was added drop by drop to reach the molar ratio of 1:15. The solution was kept under stirring for 2 h. The final mixed oxide support was obtained after drying the gel at 90 °C for 20 h on a sand bath and calcining it at 500 °C for 2 h in a muffle furnace. The addition of vanadia was done using the wet impregnation method. At room temperature (RT) the appropriate amount of vanadium precursor, $VO(acac)_2$ was dissolved in methanol. The support in a powder form was added to the solution and the mixture was agitated overnight. The material was then dried on a sand bath at 80 °C followed by heating at 120 °C for 2 h. The target amount of vanadia calculated as vanadium pentoxide $V_2O_5$ on the support was 1.5 wt%.

To discover the effect of calcination on the vanadium species, three different thermal treatments were performed for the impregnated and dried material: stagnant air calcination (in a muffle furnace), calcination under an air flow (in a tubular reactor), and calcination under $N_2$ flow (in a tubular reactor). The calcination environments for the sol-gel prepared materials were selected based on the work performed by De Jongh et al. [47–49]. Each treatment used the heating program from room temperature to 500 °C with 1 h ramp at 250 °C and the heating rate of 5 °C $min^{-1}$. The total gas flow was kept at 1 L $min^{-1}$. During the preparation of the 1.5V/SiTi(30) catalyst the support was ground, and the particle size fraction from 100 μm to 500 μm was used in the experiments.

The $TiO_2$-rich vanadia catalysts were provided by Dinex Finland and contained 3% of $V_2O_5$ on $TiO_2$ and on $TiO_2$+$SiO_2$(5%). Vanadia was added on the support using a commercial preparation method. The materials were used as powders (*in situ* methanol experiments and light-off experiments) or as washcoated metal monoliths (light-off experiments). These materials are referred as “reference catalysts” in the following chapters.

The nomenclature of the used catalysts is presented in Table 1. Since all the catalytic materials were not used in every experiment, Table 1 indicates also the experiments carried out. As some color differences indicating different vanadia species were observed after the calcination

**Table 1**
Nomenclature of the catalysts used in this work and the performance-related experiments carried out (activity-related experiments were *in situ* DRIFT experiments, oxidative dehydrogenation of methanol alone, and oxidative dehydrogenation and desulfurization of methanol-methyl mercaptan mixture).

| Support/Catalyst | Calcination environment | Nomenclature | Colour after calcination | *in situ* DRIFT | MeOH | MeOH + MM |
|---|---|---|---|---|---|---|
| **Self-made catalysts (silica-rich)** | | | | | | |
| $SiO_2$+$TiO_2$(30%) | air, stagnant | SiTi(30) | white | x | | x |
| 1.5%$V_2O_5$/$SiO_2$+$TiO_2$(30%) | air, stagnant | 1.5V/SiTi(30)$_{AS}$ | yellow | | | x |
| 1.5%$V_2O_5$/$SiO_2$+$TiO_2$(30%) | air, flow | 1.5V/SiTi(30)$_{AF}$ | yellow | x | x | x |
| 1.5%$V_2O_5$/$SiO_2$+$TiO_2$(30%) | $N_2$, flow | 1.5V/SiTi(30)$_{N2}$ | black | x | x | x |
| **Reference catalysts (titania-rich)** | | | **form** | | | |
| $TiO_2$ | air | Ti | powder | | | |
| $TiO_2$+$SiO_2$(5%) | air | TiSi(5) | powder | x | | x |
| 3%$V_2O_5$/$TiO_2$ | air | 3V/Ti | powder | | | x |
| 3%$V_2O_5$/$TiO_2$+$SiO_2$(5%) | air | 3V/TiSi(5) | powder | x | x | x |
| 3%$V_2O_5$/$TiO_2$ | air | 3V/Ti(M) | monolith | | | x |
| 3%$V_2O_5$/$TiO_2$+$SiO_2$(5%) | air | 3V/TiSi(5)(M) | monolith | | | x |

treatments, the colors are mentioned here as well.

### 2.2. Characterization

$N_2$ adsorption-desorption isotherms were measured at − 196 °C using a Micrometrics ASAP 2020 apparatus to determine specific surface areas, pore sizes and pore volumes of the materials. Before $N_2$ adsorption, the samples were degassed at 300 °C under vacuum for 2 h. The BET-BJH -methods (Brunauer-Emmett–Teller Barret-Joyner-Halenda) was used in the calculations.

To study the elemental composition of the catalyst samples X-ray fluorescence analysis (XRF) was used. A sample mass of 0.2 g was mixed with 8.5 g of flux (66% lithium tetraborate, 34% lithium metaborate) in a Pt-Au crucible followed by melting in an Eagon 2 furnace at 1150 °C. The analysis was performed with an Axios mAX x-ray fluorescence spectrometer (PANalytical). In case of vanadia containing reference catalysts the XRF analysis was performed to sample powders which were scratched from monolith catalysts. To characterize the crystalline structure of the materials, an X-ray diffractometer (XRD) PANalytical X'Pert PRO device was used. Analysis data was recorded between 2θ range of 10° and 80°, with a step size of 0.040°. X-ray photoelectron spectroscopy (XPS) analysis was carried out by a Thermo Fischer Scientific ESCALAB 250Xi instrument equipped with a monochromatic Al Kα (1486.6 eV) radiation to excite photoelectrons. The fresh sol-gel prepared samples were put on an indium substrate and placed inside a vacuum chamber. The binding energy was normalized with respect to the position of the C1s peak at 284.8 eV and the Smart function was used for the background reduction. The data analysis was performed by fitting the signals with the mixed Gaussian-Lorentzian function using the Thermo Avantage -software. The spectra recorded covered the C1s, O1s, Si2p, Ti2p, and V2p photoelectron peaks. The XPS measurement for the reference catalysts were performed at MAX IV Laboratory (Lund, Sweden) with the APXPS end station of the HIPPIE beamline which is described elsewhere [50]. The samples were prepared by dilution of approximately 100 mg of the catalyst powder into 5 mL of ethanol, and spin-coated onto a gold foil. The Au 4f7/2 core level from the gold foil was used for energy calibration at 84.0 eV. A combination of a linear with a Shirley background was subtracted from the spectra and fitted with an Igor Pro 6 software with mixed- Gaussian-Lorentzian function.

Temperature programmed reduction ($H_2$-TPR) and $NH_3$-desorption ($NH_3$-TPD) were performed using an AutoChem II 2920 equipped with a thermal conductivity detector (TCD). In $H_2$-TPR, a ~40 mg sample was pre-treated in an oxygen ($O_2$) flow (50 mL min$^{-1}$) for 30 min at 500 °C and cooled down to room temperature. Then, the excess $O_2$ was removed by flushing the sample with helium (He) for 30 min. The $H_2$-TPR measurement was carried out under 10% hydrogen ($H_2$) in argon (Ar) up to 500 °C with a heating rate of 10 °C min$^{-1}$. In the $NH_3$-TPD, a ~40 mg sample was pre-treated in a He flow (50 mL min$^{-1}$) for 30 min at 450 °C and cooled down to 100 °C. $NH_3$ adsorption was performed under 5% $NH_3$ in He at 100 °C for 60 min after which the sample was flushed with He for 30 min to remove excess $NH_3$. Finally, temperature was raised from 100 °C to 500 °C with the heating rate of 10 °C min$^{-1}$ and concentration of the desorbed ammonia was determined using a TCD detector. In the desorption step, He (50 mL min$^{-1}$) was used as a carrier gas.

A (scanning) transmission electron microscope ((S)TEM) Jeol JEM-F200 together with an energy dispersive spectrometer (EDS) Jeol Dual EDS for F200 was used to study the sol-gel prepared 1.5%$V_2O_5$/$SiO_2$-rich catalysts and the 3%$V_2O_5$/$TiO_2$-rich reference catalysts. The morphology and structure of the catalysts were studied by TEM together with selected area electron diffraction (SAED). The distribution of vanadium on the catalyst support was studied by STEM-EDS. (S)TEM samples were prepared by crushing a catalyst powder between microscope slides and dispersing the powder with isopropanol onto a holey-carbon-coated copper grid. A carbon contamination disturbed the STEM-EDS analysis of the 3$V_2O_5$/$TiO_2$-rich reference catalysts and thus, they were plasma-cleaned prior to the STEM studies.

A Timegated® Pico Raman spectrometer with a pulsed excitation laser (532 nm) and a time-resolved single-photon counting detector (spectral resolution ~5 cm$^{-1}$) was used in *in situ* Raman measurements. The spectrometer was equipped with an *in situ* cell (Linkam CCR1000) in which the temperature and gas conditions were controlled during the measurement. The spectra were collected at the Raman shift range from 100 to 2100 cm$^{-1}$ at temperatures 23 °C (RT), 100 °C, 300 °C, 400 °C, 500 °C and 600 °C. Air flow of 50 mL min$^{-1}$ was used in a flow-through catalyst holder. Laser power of Raman was adjusted to 75% to avoid laser-induced changes in the material. The data was background corrected using a tailormade Shsqui Matlab® based software.

### 2.3. In situ DRIFT studies

The *in situ* DRIFT experiments were performed with Bruker Vertex V 80 equipped with an MCT detector and a Harrick high temperature diffuse reflectance IR gas cell fitted with $CaF_2$ windows. The spectra were recorded with a resolution of 4 cm$^{-1}$ using 200 signal-averaged scans. A calibrator (Gasmet Technologies, Finland) equipped with a mass flow meter, a syringe pump and an evaporator unit were used for the methanol feed. The gas lines leading to and from the DRIFT gas cell were heated up to 180 °C to prevent condensation of vapours. The DRIFT cell gas outlet was connected to an FTIR Gas analyzer Cr-2000 (Gasmet Technologies, Finland) for simultaneous exit gas analysis. The schematic of the set-up is presented in Fig. 1.

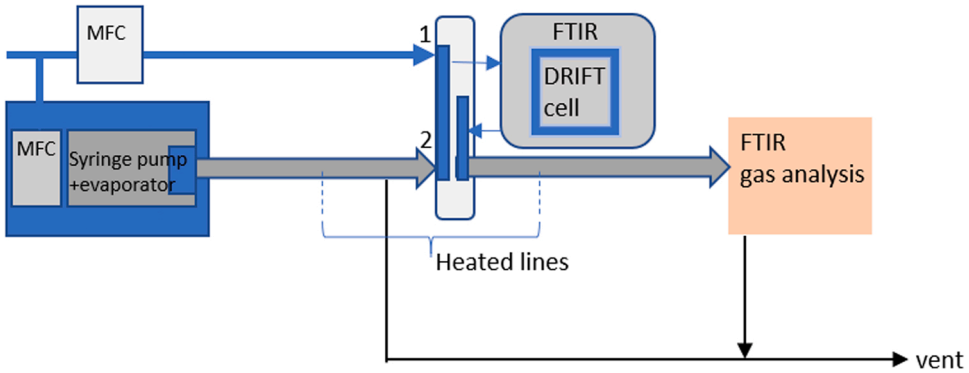


**Fig. 1.** Experimental set-up used in the *in situ* methanol oxidative dehydrogenation experiments ([1] synthetic air flow, [2] flow of 2000 ppm methanol in synthetic air).

Prior to *in situ* experiments, the catalyst was heated up to 200 °C for 30 min in a synthetic air flow (20/80 $O_2/N_2$, 200 mL $min^{-1}$). The aim of the pre-treatment was to dehydrate the catalyst surface without affecting significantly the vanadia species. After the pre-treatment, the following temperature steps were used: 100 °C, 200 °C *etc.* until 500 °C. At each temperature step, the sample was purged with synthetic air (200 mL $min^{-1}$) for 15 min, after which ~2000 ppm methanol with synthetic air was introduced into the DRIFT cell for 30 min. Then, the sample was purged with air for ~5 min. Three DRIFT spectra were taken at each temperature: before, during and after methanol introduction. The air flow rate of 200 mL $min^{-1}$ was used in each heating and constant temperature step. The $N_2$ calcined material was not pre-treated before the methanol adsorption experiment to minimize re-oxidation of the material.

### 2.4. Catalytic experiments

The catalytic activity experiments (light-off experiments) were performed in a tubular quartz reactor. The experimental set-up presented in our previous work [14] was modified slightly: experiments were performed using synthetic air and all the gas lines after the evaporator (heated to ~70 °C) were heated up to 180 °C to avoid adsorption or condensation inside the equipment lines.

The experiments with powder form catalysts were conducted using a catalyst mass of 100 mg. The size of monolith was adjusted so that it contained the same mass of catalyst (100 mg) washcoated on the metal substrate. When comparing the support powders, the SiTi(30) support was ground to avoid the impact of different particle sizes on the results. Internal diffusion is not affecting the experimental results markedly when the particle size remains below 500 μm [51]. The GHSVs during the experiments were 94,000 $h^{-1}$ for the powder-form catalysts and 41,000 $h^{-1}$ for the monoliths. The feed concentration in each sulfur-containing methanol oxidation experiment was 500 ppm of methanol and 500 ppm of methyl mercaptan. The total gas flow was 1 L $min^{-1}$. The oven temperature was raised from room temperature to 500 °C with the heating rate of 5 °C $min^{-1}$. Selected materials were also investigated in the oxidation of 1000 ppm of methanol to discover the effect of the addition of sulfur into the gas feed on the catalyst performance. The outlet gas composition was analyzed using a Gasmet FTIR Cr-2000 analyzer equipped with an MCT detector. The following compounds were analyzed: carbon dioxide $CO_2$, carbon monoxide CO, nitrogen monoxide NO, nitrogen dioxide $NO_2$, nitrous oxide $N_2O$, sulfur dioxide $SO_2$, sulfur trioxide $SO_3$, methane $CH_4$, formaldehyde $CH_2O$, methyl mercaptan $CH_4S$, dimethyl sulfide $C_2H_6S$, dimethyl disulfide $C_2H_6S_2$, formic acid $CH_2O_2$ and methanol $CH_4O$.

## 3. Results and discussion

### 3.1. Characterization of sol-gel prepared silica-rich catalysts

One aim of the characterization of the 1.5V/SiTi(30) catalysts was to discover effects of calcination treatments. Specific surface areas, pore volumes and pore sizes of these catalysts are given in Table 2 with the catalyst compositions calculated as oxides from the measured XRF results.

The sol-gel prepared mixed oxide support reached relatively high specific surface area of 490 $m^2$ $g^{-1}$. The target $TiO_2$ amount of the SiTi support (30%) was achieved reasonably well. The vanadia amount of each catalyst was slightly below the target (1.5%). Addition of vanadia decreased the specific surface area of the catalysts by around 100 $m^2$ $g^{-1}$. In these catalysts, vanadia surface density (~0.2 V atoms $nm^{-2}$) does not reach the monolayer coverage. It has been determined before that the monolayer for vanadium on $TiO_2$ equals to surface density of about 7.9 V atoms $nm^{-1}$ and for the $SiO_2$ support the maximum dispersed coverage is reached at around 2.6 V atoms $nm^{-1}$ [52,53].

The XRD patterns for the sol-gel prepared catalysts, presented in the supplementary material (Fig. S1), showed a broad hump at 2θ value ~25° for all the materials indicating an amorphous state originating from the high $SiO_2$ content. No crystalline $TiO_2$ or vanadia phases were visible from the diffractograms. According to the result, the amorphous structure is similar despite of different calcination treatments, and vanadia seems to be highly dispersed in these materials. Similar findings have been presented by Liu et al. [54].

The results of temperature programmed reduction ($H_2$-TPR) and temperature programmed ammonia desorption ($NH_3$-TPD) are presented in Fig. 2. The $H_2$-TPR curves do not show significant consumption of $H_2$ in the temperature range from 200 °C to 500 °C. It is known that

**Table 2**
BET-BJH and catalyst composition (calculated from XRF) results for the silica-rich catalysts.

| Catalyst | Surface area [$m^2$ $g^{-1}$] | Pore volume [$cm^3$ $g^{-1}$] | Pore size [nm] | V surface density [V atoms $nm^{-2}$] | XRF $V_2O_5$ [%] | XRF $SiO_2$ [%] | XRF $TiO_2$ [%] |
|---|---|---|---|---|---|---|---|
| SiTi(30) | 490 | 0.30 | 2.4 | – | – | 65.8 | 29.9 |
| 1.5V/SiTi(30)$_{AS}$ | 390 | 0.25 | 2.5 | 0.20 | 1.2 | 62.8 | 28.2 |
| 1.5V/SiTi(30)$_{AF}$ | 400 | 0.26 | 2.5 | 0.21 | 1.2 | 66.2 | 29.7 |
| 1.5V/SiTi(30)$_{N2}$ | 390 | 0.25 | 2.5 | 0.20 | 1.1 | 64.1 | 29.1 |

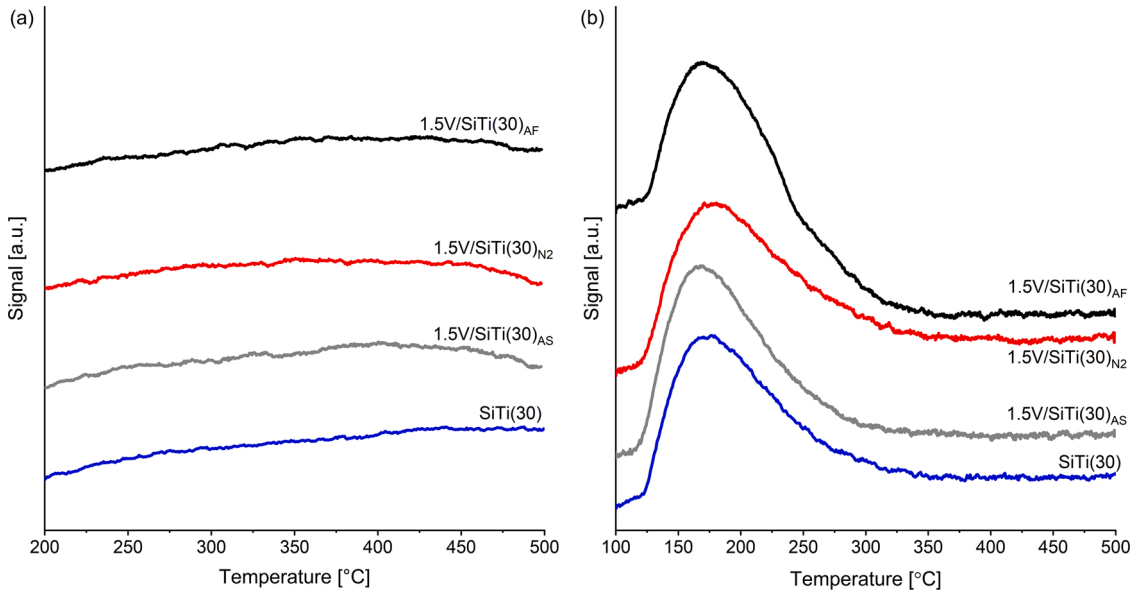


**Fig. 2.** (a) $H_2$-TPR and (b) $NH_3$-TPD profiles of 1.5V/SiTi(30) catalysts collected in the temperature range of 100 °C to 500 °C with the heating rate of 10 °C $min^{-1}$.

$TiO_2$ reduces at around 550 °C [55] and $SiO_2$ can be considered as a non-reducible support [56]. Incorporation of silica in titania in a mixed oxide is expected to stabilize titania. Vanadia species on $TiO_2$ have reported to reduce at around 500 °C and on $SiO_2$ at around 600 °C [57, 58]. The absence of vanadia reduction peak may arise from the quality and quantity of vanadia species, but also from the stabilization of the oxide species due to the support. The TPR experiments were not carried out at higher temperatures, since the maximum temperature for the catalytic experiments was 500 °C. Based on the results, it is not expected that silica-titania support goes through any significant oxidation/reduction cycles during the catalytic experiments.

The temperature programmed desorption of $NH_3$ was measured to quantify the total amount of acid sites. The results of SiTi(30) supported vanadia catalysts indicate mainly the presence of weak acid sites, that are able to retain $NH_3$ adsorbed until about 300 °C. The maximum of $NH_3$ desorption peak is observed at about 170 °C with the air calcined catalysts and the support, and with the $N_2$ treated catalysts at slightly higher temperature. The total acidity is the highest for the air flow calcined catalyst, 1.5V/SiTi(30)$_{AF}$ (687 μmol $g^{-1}$), followed by 1.5V/SiTi (30)$_{N2}$ (627 μmol $g^{-1}$). The lowest total acidity is observed for the

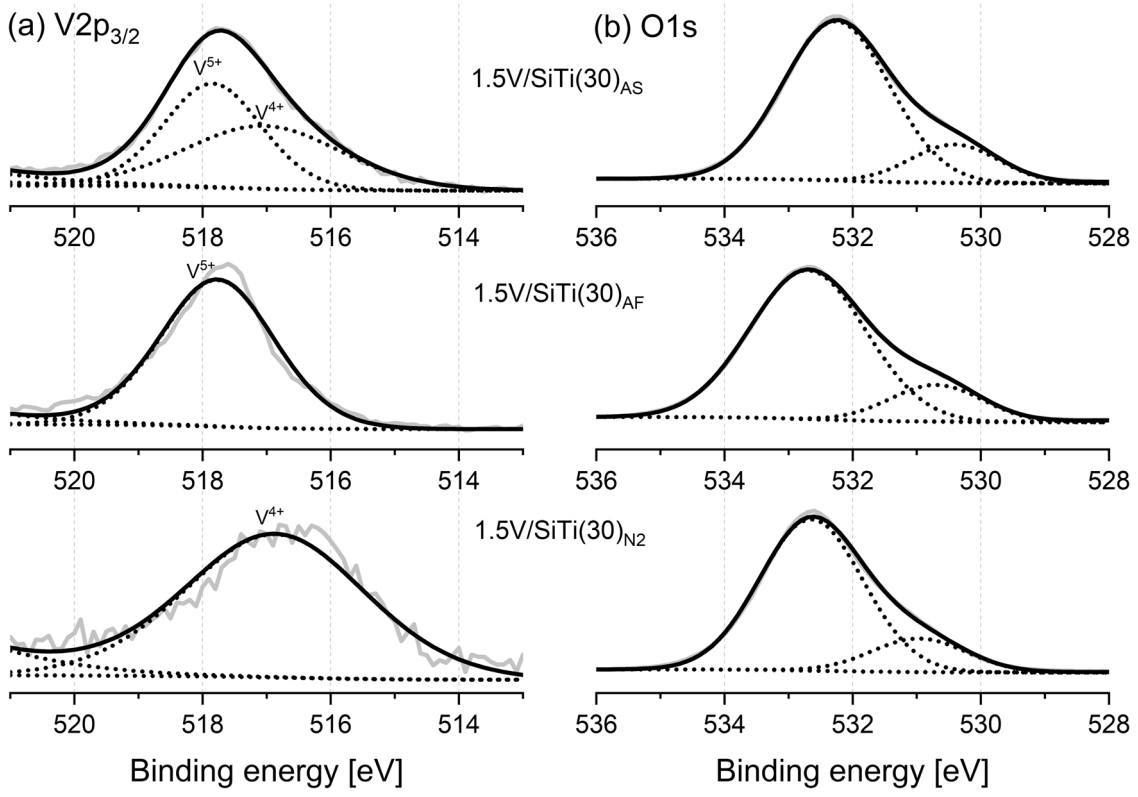


**Fig. 3.** Electron spectra of 1.5V/SiTi(30)$_{AS}$, 1.5V/SiTi(30)$_{AF}$, and 1.5V/SiTi(30)$_{N2}$ (calcined at 500 °C) covering (a) V2$p_{3/2}$ and (b) O1s photoelectron peaks.

catalyst calcined in stagnant air in a muffle furnace (590 μmol $g^{-1}$). For the silica-titania support, SiTi(30), the total acidity is 618 μmol $g^{-1}$. Dong et al. [59] connected the influence of oxygen amount used during calcination on the surface acidity and found that the total acidity is the lowest for a catalyst calcined in an oxygen free environment. This is in accordance with lower total acidity of the $N_2$-calcined catalyst compared with the catalyst calcined in an air flow. Dong et al. [59] further noted that the ratios of $V^{4+}/V^{5+}$ and $V^{4+(3+)}/V^{5+}$ affect the strength of acidity for the $V_2O_5$–$WO_3$/$TiO_2$ catalysts in such a way that the more the catalyst contains lower oxidation states of vanadium, the stronger the acid sites are. It is considered that methanol adsorbs on the acid sites to form a methoxy intermediate. The further reaction, and formation of different products is then dependent on the prevailing reaction mechanism. In the presence of high amounts of acid sites, oligomeric products are observed. The formation of formaldehyde requires redox sites, which lead to the Mars van Krevelen –type of a reaction mechanism. Although acid sites are required for methanol adsorption, their excessive amount may lead to the formation of oligomeric products, such as DME, DMS and DMDS, in the expense of formaldehyde Damyanova et a. [83].

The XPS results for the 1.5%V/SiTi(30) catalysts are presented in Fig. 3. Based on the XPS study the oxidation state of vanadium on the silica-titania support was determined using the $V2p_{3/2}$ core level spectra [60,61]. The determination of vanadium oxidation states using the conventional XPS should be done with caution, since the reduction of vanadium species are observed under the ultra-high vacuum (UHV) conditions [62–65].

The V2p and O1s regions were fitted together. The following constrains were used in the fitting: $V2p_{1/2}$ - $V2p_{3/2}$ splitting 7.50 + /- 0.5 eV, distance between $V^{5+}$ and $V^{4+}$ (in $V2p_{3/2}$) is 1 + /- 0.2 eV and Lorenz-Gaussian ratio is 30% [66]. The V2p spectra show a two-peak structure ($V2p_{3/2}$ and $V2p_{1/2}$) [61,67]. Due to the low intensity of the $V2p_{1/2}$ signal, only $V2p_{3/2}$ is shown in Fig. 3. The deconvolution of $V2p_{3/2}$ reveals the existence of vanadium oxidation states of 4+ and 5+ for $1.5V/SiTi(30)_{AS}$. For a catalyst calcined in an air flow ($1.5V/SiTi(30)_{AF}$), the results indicate the existence of $V^{5+}$ and for the $N_2$ calcined sample, the existence of only $V^{4+}$ is evident [68,69]. This result shows that calcination under stagnant air does not result in a homogeneous composition of oxidation states for vanadium, and that inert gas atmosphere leads to a lower oxidation state of vanadium, as expected. Furthermore, the result supports the earlier indication related to the oxidation state ratios and strength of acidity, since slightly higher and wider $NH_3$ desorption temperature range was observed for the $N_2$ calcined catalyst.

The O1s signal of the catalysts could be deconvoluted into two peaks: a major one at ~532.7 eV and a minor one at ~530.7 eV. The metal oxygen bonds appear at around 528.1–531 eV, and the quite wide peak observed at 530.5 eV could mainly be related to oxygen species in $TiO_2$, but also partly to vanadia. The second peak appearing at ~532.7 eV is in the region where oxygen in $SiO_2$ is observed, however, hydroxyl oxygen (-OH) may appear in the same region where the second peak is fitted. [70].

All the binding energy values for V2p, O1s, Si2p and Ti2p and the XPS spectra of silica and titania are included in the supplementary material (Table S1 and Fig. S2). The deconvolution of the Si2p spectra revealed one peak at the binding energy values between 103.0 and 103.4 eV representing the Si oxidation state of 4+ . Stakheev et al. [71] have observed earlier the presence of Si2p peaks between 102.5 and 104.1 eV depending on the Ti amount in the sample. $TiO_2$ had a two-peak structure; the binding energy values for $Ti2p_{3/2}$ were approximately the same for all the samples (459.2–459.6 eV) and $Ti2p_{1/2}$ were observed between 464.9 and 465.4 eV. Additionally, a $TiO_2$ shake-up peak was located at ~472 eV. The $Ti2p_{3/2}$ peaks are slightly shifted towards a higher binding energy, which may originate from the mixed oxide structure. Ti was observed to have an oxidation state of 4+ .

The TEM images together with the SAED patterns and the STEM dark field (DF) images together with the EDS line analyses of the fresh 1.5V/SiTi(30) catalysts with different calcination environments are presented in Fig. S5 in the supplementary material. The TEM images and SAED patterns show an amorphous structure agreeing with the XRD results. The distribution of Si, Ti, and V is similar in all the catalysts (oxygen is excluded from the images). Even if the energies of the Ti Kβ (4.930 keV) and V Kα (4.948 keV) peaks are close to each other, titanium and vanadium could be distinguished in the STEM-EDS line analyses. Vanadium seems to exist preferably on the same locations with titanium agreeing with the findings of Albonetti et al. [72] and Quaranta et al. [73] who present that vanadia does not interact significantly with silica.

The Raman spectra between 150 and 1200 $cm^{-1}$ for the SiTi(30) and 1.5V/SiTi(30) catalysts are presented in Fig. 4 under fully dehydrated conditions at 500 °C. Table S2 in the supplementary material presents the Raman band identifications for $V_2O_5$, $SiO_2$ ja $TiO_2$.

For the SiTi support, the main spectral features are located at ~1085, 926, 890, 813, 640, 475–458 and 152 $cm^{-1}$. In general, silica was not expected to give a strong Raman signal due to its amorphous nature observed in XRD. In addition, silica exhibits weaker Raman bands than titania due to an ionic character of the Si-O bonds [52]. The most interesting peaks of the spectrum of the SiTi support include a feature at 458–475 $cm^{-1}$ that can be assigned to the Si-O-Si bending mode. The peak is wide due to the insertion of Ti with the silica network, which leads to distortion of the $SiO_4$ tetrahedra. The left side shoulder of the peak at around 480 $cm^{-1}$ may also indicate the defects in the silica network. Silica gives also rise to the peak observed at 1085 $cm^{-1}$ (υ (Si-O-Si) asymmetric stretching). The peak at 152 $cm^{-1}$ is related to the anatase-phase of $TiO_2$, however, other titania peaks (related to anatase or rutile phases) cannot be clearly distinguished from the spectrum. [74] The peaks observed at around 880–950 $cm^{-1}$ have been confirmed earlier to originate from Ti-O-Si bonds [75], which feature is visible also in the SiTi spectrum. Another indication of the Ti-O-Si structure would be visible at around 1100 $cm^{-1}$, but it is superimposed with the Si-O-Si asymmetric stretching [74]. These results indicate that silica and titania in the support represent a mixed oxide structure.

Raman spectral features of the vanadia-loaded catalysts at ~1030 $cm^{-1}$ and 920–950 $cm^{-1}$ are characteristic of the supported vanadia species. The peak observed at 1031 $cm^{-1}$ is related to the V═O stretching of the monovanadate species that are predominant at lower surface coverages of vanadia. For single oxide $TiO_2$, this peak has been reported to appear at 1025 $cm^{-1}$ and for $SiO_2$ at 1039 $cm^{-1}$ [52]. Based on this information, monovanadate species appear preferably on titania in this case. Peaks indicating monovanadate species are clearer for nitrogen and stagnant air -calcined samples, while in the case of air flow calcined catalyst the V═O peak is less intense. The $N_2$ calcined catalyst also shows presence of peaks at around 813–890 $cm^{-1}$ related to multiple vibrations of the V-O-V and V-O-support bonds of polymerized surface vanadia species. Equal amounts of polymerized vanadia species were not observed for the other catalysts although a clear peak appears at 890 $cm^{-1}$. The polymerized vanadia species are not typically observed in the case of a single oxide $SiO_2$ support, but the presence of titania in the mixed oxide structure seems to make it possible in this case. Similarly, $V_2O_5$ crystals are not typically present at low surface loadings of vanadia, however, a small peak at 994 $cm^{-1}$ indicating $V_2O_5$ is observed in this case for a catalyst calcined in stagnant air. This result indicates a lower dispersion degree of vanadia on the surface of the stagnant air calcined catalyst. [76] In general, it seems that slightly different vanadia species are formed on the TiSi support during different calcinations of the catalyst.

The Raman spectra at hydrated and non-hydrated conditions (from RT to 600 °C, excluding 200 °C) for the sol-gel prepared vanadia catalyst are presented in the supplementary material (see Fig. S7, S8 and S9). The figures show that the intensity of the terminal V═O stretching increases with increasing the temperature. This is most probably due to hydrolysis of the V═O bond by atmospheric moisture during the storage of the catalysts, which decreases when increasing the temperature [41]. In

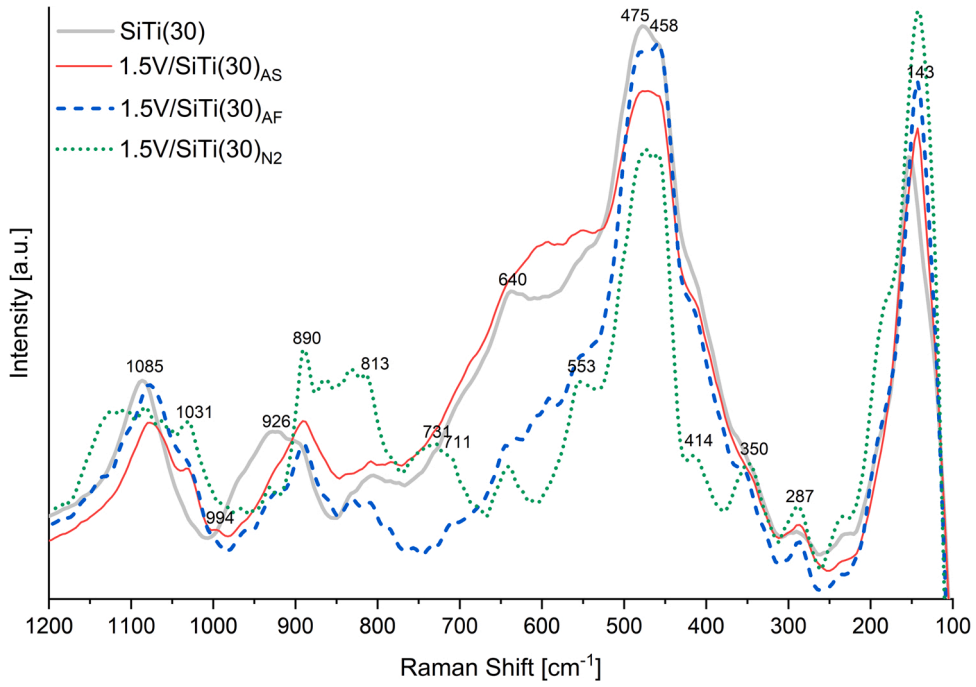


**Fig. 4.** Raman spectra of SiTi(30), 1.5V/SiTi(30)$_{AS}$, 1.5V/SiTi(30)$_{AF}$ and 1.5V/SiTi(30)$_{N2}$ measured at 500 °C.

addition, the peak indicating the presence of $V_2O_5$ in the 1.5V/SiTi (30)$_{AS}$ catalyst decreases when increasing the temperature up to 600 °C. The results show that the relative amounts and types of the vanadia species change upon heating the catalyst in air. This is also expected to occur during the catalytic experiments.

### 3.2. *In situ* oxidative dehydrogenation of methanol over silica-rich catalysts

*In situ* DRIFT experiments were carried out to study especially the C-H stretching region (adsorbed methoxy intermediates) between 2700 and 3000 cm$^{-1}$ at different temperatures. The *in situ* DRIFT spectra of

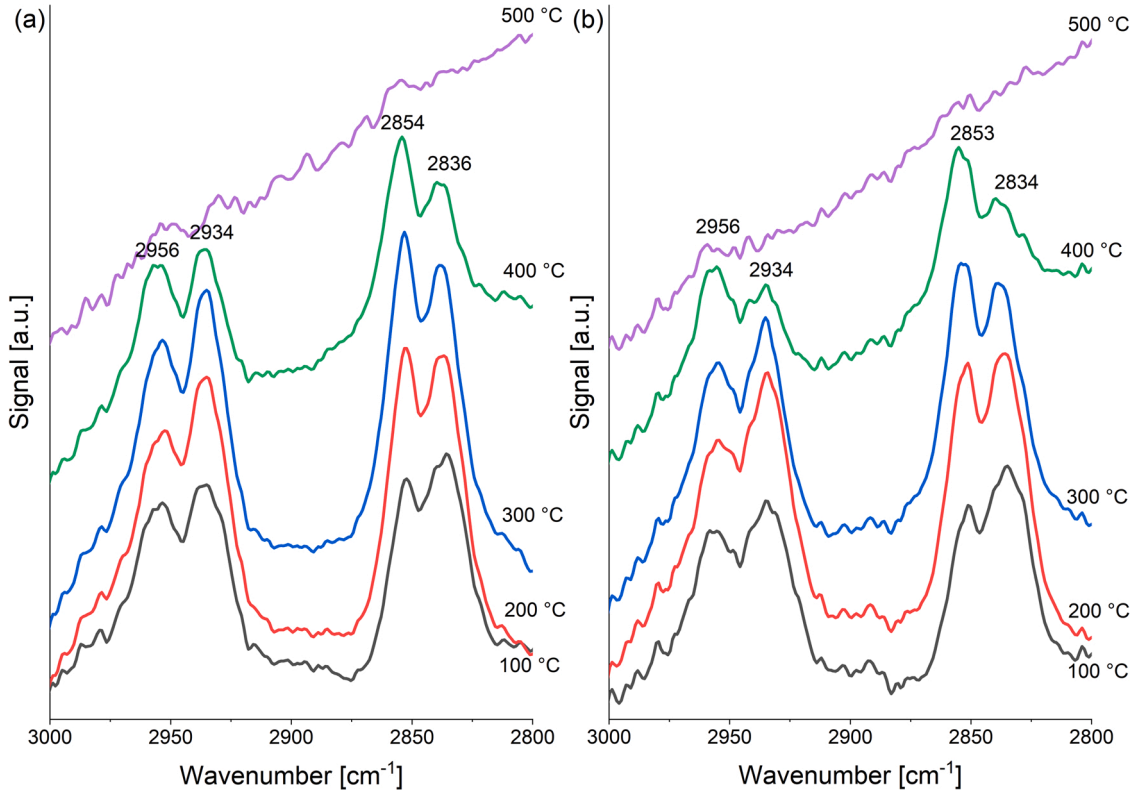


**Fig. 5.** *In situ* DRIFT spectra in the C–H stretching region for (a) SiTi(30) and (b) 1.5V/SiTi(30)$_{AF}$ catalysts from RT to 500 °C. Spectra taken after ~5 min of an air flow after a 30 min methanol feed (~2000 ppm in air) to the DRIFT cell.

adsorbed methoxy species are presented in Fig. 5 for the support SiTi (30) and for 1.5V/SiTi(30)$_{AF}$ calcined in an air flow. Previous studies [22,77] present the methanol adsorption for single oxide supports ($SiO_2$, $TiO_2$). The catalysts calcined under air and $N_2$ flows were selected to investigate further the effects of the calcination atmosphere and the observed structural differences on materials' performance. For the mixed SiTi(30) support, the methoxy vibrations consist of two bands in the Fermi resonance located at around 2836 and 2934 $cm^{-1}$ (Ti-$OCH_3$) and 2854 and 2956 $cm^{-1}$ (Si-$OCH_3$). The vibrations are located at slightly higher values than those reported for single oxide $TiO_2$, and lower than those reported for single oxide $SiO_2$ (See also supplementary material Table S3) [22]. This is due to the mixed oxide structure of the support.

After the addition of vanadia, the peak positions of Ti-$OCH_3$ and Si-$OCH_3$ remain at similar locations when taking the spectral resolution into account. The V-$OCH_3$ vibrations according to Burcham et al. [22] appear at 2832 and 2936 $cm^{-1}$, which makes the distinction between the Ti-$OCH_3$ and V-$OCH_3$ difficult with the 1.5% vanadia catalysts. A weak shoulder at 2970–2983 $cm^{-1}$ is assigned to $\nu_{as}(CH_3)$. The band at ~2900 $cm^{-1}$ is assigned to an overlapping mode $2\delta_{as}(CH_3)$ from a second methoxy overtone band [22]. Fig. S10 and Fig. S11 in the supplementary material show the deconvolution of methoxy peaks at 100 °C, 300 °C and 500 °C.

Fig. 6a presents the *in situ* DRIFT spectra of adsorbed methoxy species for 1.5V/SiTi(30)$_{N2}$. In Fig. 6b, the relative gas-phase concentrations of methanol (MeOH), formaldehyde (FO), CO and $CO_2$ at the outlet of the experimental cell at constant temperatures are presented. The peak surface area indicating the amount of methoxy species increases at temperatures up to 300 °C. A decrease in methanol gas-phase concentration is observed at 200 °C. The formation of formaldehyde (FO) begins at 300 °C reaching the maximum at 400 °C, after which the concentration decreases due to the oxidation reactions. At 500 °C, only a small amount of Si-bonded methoxy species is observed on the catalyst surface. At this temperature, no more methanol is observed in the gas analyses. Methoxy adsorption on silica seems to be stronger. This is most evident in the case of $N_2$ calcined V/SiTi(30) as Si-$OCH_3$ is clearly visible at 500 °C. This catalyst has also the highest amount of monomeric and polymeric vanadium species at 500 °C and it had the lowest but strongest acidity. The reaction gas analysis results are presented for SiTi(30) and V/SiTi(30)$_{AF}$ in the supplementary material (Fig. S13).

Table 3 presents the methoxy peak positions and selected peak surface areas of the SiTi(30) support as well as the nitrogen and air flow calcined catalysts. The intensity of both Si-$OCH_3$ and Ti-$OCH_3$ bands first increases with temperature and then decreases. The maxima are observed at 200 °C and 300 °C, respectively. In the case of 1.5V/SiTi (30)$_{AF}$, the methoxy species are not anymore observed at 500 °C, while for 1.5V/SiTi(30)$_{N2}$ and SiTi(30) they still exist. The methanol conversion is not complete at 500 °C with 1.5V/SiTi(30)$_{AF}$ (see supplementary Fig. S13), while with 1.5V/SiTi(30)$_{N2}$ it is. Formaldehyde formation is highest with 1.5V/SiTi(30)$_{N2}$. In this type of reaction, the adsorption step is the typical rate determining reaction step, while surface reaction is very rapid [22]. In excess air, methanol adsorbs on the support as methoxy species, and leads to the formation of formaldehyde, but excess oxygen also enables further oxidation of methanol and formaldehyde to $CO_2$ and CO. Oxidative dehydrogenation of methanol to formaldehyde has been demonstrated to follow the Mars-van Krevelen mechanism where lattice oxygen from the solid is used for oxidation of the reactant [78]. The Mars-van Krevelen reaction mechanism assumes two independent steps: first $H_2$ is abstracted from the adsorbed reactant forming water with the surface oxygen atom, and in the second step, the active site is re-oxidized by molecular oxygen [79]. The hydrogen abstraction from methoxy groups is proposed to be the rate-determining step of surface reaction and it suggests that V plays an important role in this step. V is also expected to speed the redox cycle. In the case of 1.5V/SiTi (30)$_{AF}$, the further oxidation appears at higher extent than in the case of 1.5V/SiTi(30)$_{N2}$. It is clear, that vanadia enhances formaldehyde

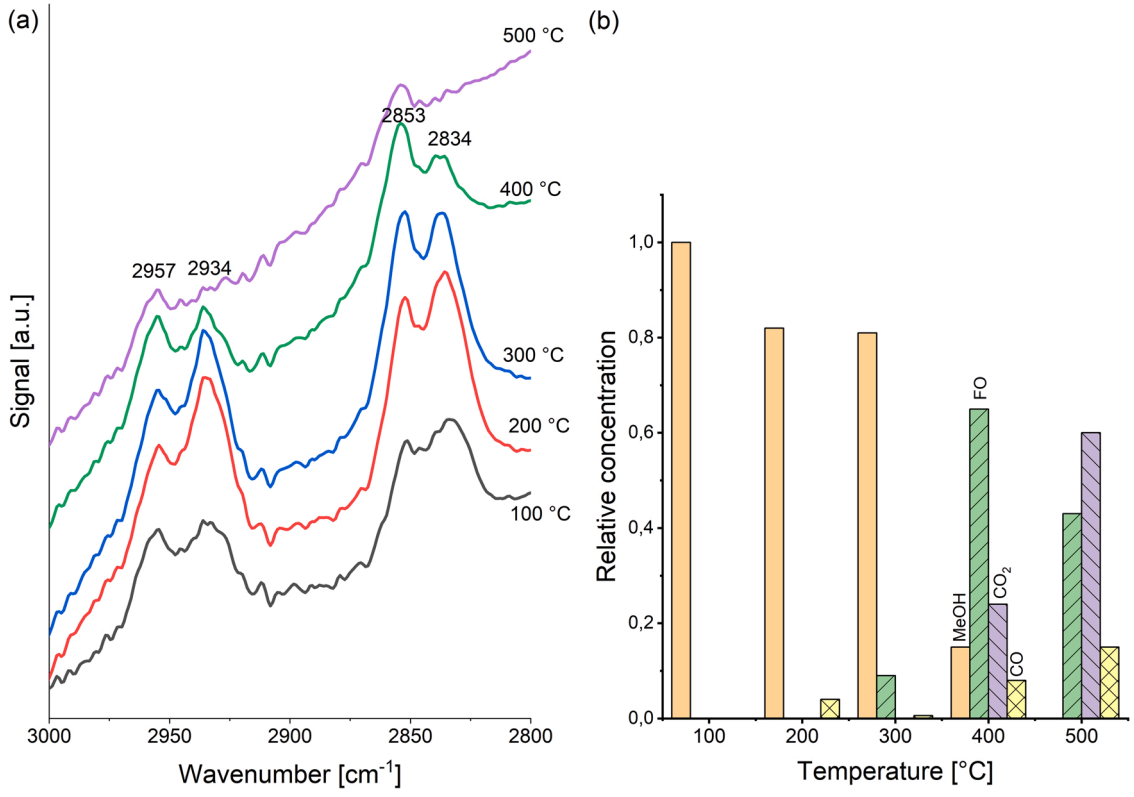


**Fig. 6.** *In situ* (a) DRIFT spectra in the C–H stretching region of V/SiTi(30)$_{N2}$ from RT to 500 °C, the spectra taken under an air flow (~5 min) after a 30 min methanol feed (~2000 ppm in air) to the DRIFT cell. (b) Relative gas concentrations measured during *in situ* methanol adsorption.

**Table 3**
Observed peak wavenumbers of adsorbed methoxy species on the SiTi(30) catalysts during methanol reaction at temperatures from 100 °C to 500 °C.

| Temperature | SiTi (30) | | 1.5V/SiTi (30)$_{AF}$ | | 1.5V/SiTi (30)$_{N2}$ | | pure oxides[22] | |
|---|---|---|---|---|---|---|---|---|
| | Si-OCH$_3$ | Ti-OCH$_3$ | Si-OCH$_3$ | Ti-OCH$_3$ | Si-OCH$_3$ | Ti-OCH$_3$ | Si-OCH$_3$ | Ti-OCH$_3$ |
| Peak position (cm$^{-1}$) at 100 °C | 2854<br>2956 | 2836<br>2934 | 2853<br>2957 | 2834<br>2934 | 2853<br>2957 | 2834<br>2934 | 2858<br>2960 | 2825<br>2924 |
| | Peak surface area | | | | | | | |
| 100 °C | 5.40 | 7.16 | 4.95 | 8.49 | 3.12 | 4.77 | | |
| 200 °C | 8.85 | 8.84 | 8.36 | 12.51 | 4.82 | 9.56 | | |
| 300 °C | 9.10 | 11.34 | 8.75 | 11.51 | 5.18 | 9.03 | | |
| 400 °C | 6.32 | 4.06 | 6.14 | 4.19 | 3.99 | 5.11 | | |
| 500 °C | 1.95 | 1.80 | * | * | 1.92 | 1.87 | | |

* not detected

production. Based on the results presented in Fig. S8, the amount of polymeric vanadia species decreases radically starting at 400 °C in the case of 1.5V/SiTi(30)$_{AF}$, while the catalyst calcined under nitrogen can retain higher amounts of polymeric vanadium species until 500 °C. This may explain the higher formaldehyde production observed for the nitrogen calcined catalyst, since monomeric and polymeric vanadium species have been reported to be most active in the reaction in concern [10,80].

### 3.3. Characterization of titania-rich reference catalysts

The titania-rich reference catalysts contained 5% of silica and 3% of vanadia. The specific surface areas of the TiSi catalyst are significantly lower than those of the SiTi catalyst (See Table 4). Since the vanadium loading is higher compared to the sol-gel prepared SiTi catalysts, vanadium surface density is significantly higher, however, the densities stay below the monolayer coverage.

The X-ray diffraction (XRD) patterns for the titania-rich reference materials are shown in Fig. 7. The XRD results did not show the peaks corresponding to $V_2O_5$ (for example, 2θ= 20.26) with the $V_2O_5$-loading of 3%. The XRD patterns are identified to 2θ values of anatase $TiO_2$ (JCPDS 00–001–0562). Anatase peaks at 36.85, 38.57 and 76.01 are less intense in silica containing catalysts due to amorphous silica [81]. The sol-gel prepared SiTi materials are highly amorphous with a high specific surface area, while the reference materials TiSi and Ti are crystalline materials with lower specific surface areas. The vanadium surface density in the titania-rich TiSi is about 12 times higher than in the silica-rich SiTi catalysts.

The results of temperature programmed reduction ($H_2$-TPR) and temperature programmed ammonia desorption ($NH_3$-TPD) for 3V/Ti and 3V/TiSi(5) are presented in Fig. 8. A strong $H_2$ consumption between 350 and 420 °C indicates easier reduction of the TiSi(5) supported catalysts. The related hydrogen consumption was equal to what is theoretically required to reduce all the vanadia from oxidation state 5+ to 3+ oxidation state. It also appears at lower temperature range than expected based on Makowski et al. [57] and Xiao et al. [58]. TiSi(5) supported catalysts are significantly less acidic than the SiTi(30) catalysts.

The APXPS results for the 3V/Ti and 3V/TiSi(5) catalysts were measured under near-ambient conditions to minimize vanadium reduction during the measurement, and are presented in Fig. 9 and Fig. 10 covering a selected region of O1s and V2p$_{3/2}$. For both the Ti and

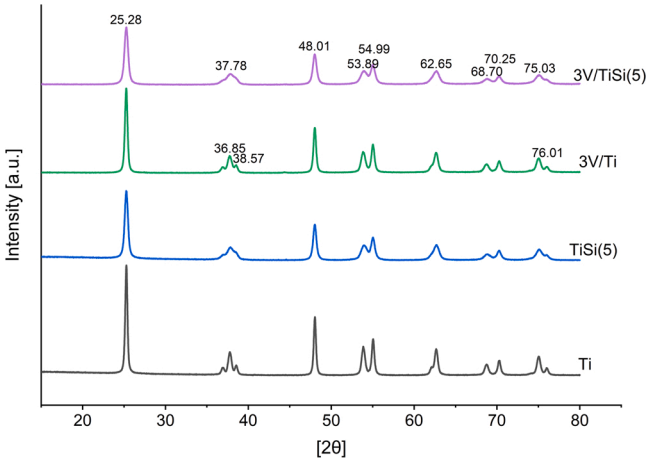


**Fig. 7.** XRD patterns of titania-rich catalysts calcined at 500 °C.

TiSi(5) supported vanadia catalysts, only the oxidation state of 4+ is observed for vanadium. The peak positions for each catalyst are presented in Table S1 in the supplementary material. The O1s signal of the titania-rich catalyst can be deconvoluted into three peaks: the major ones at 532.63 eV ($SiO_2$) and 530.32 eV ($TiO_2$ and $V_2O_5$) and a minor one at 531.71 eV (-OH). The O1s spectrum of the 3 V/Ti catalyst can be deconvoluted into two peaks: 530.39 eV indicating $TiO_2$ and $V_2O_5$ and 532.31 eV related to -OH. The spectra of silica and titania are included in the supplementary material (Fig. S3 and Fig. S4). The oxidation state of 4+ was observed for both Si and Ti. The binding energy values of 3V/TiSi(5) for Ti2p$_{3/2}$ are slightly shifted to higher binding energy values indicating a possible interaction with silica.

The TEM images together with the SAED patterns and the STEM DF images together with the EDS line analyses for 3V/Ti and 3V/TiSi(5) are presented in Fig. S6 in the supplementary material. The SAED patterns show crystalline rings from the tetragonal $TiO_2$ anatase phase (JCPDS 00–021–1272) in both catalysts. Spots from $V_2O_5$ were not observed reliably. These findings agree with the XRD results. In the SAED patterns of the 3V/TiSi(5) sample, possible diffuse rings from amorphous $SiO_2$ were challenging to detect because of the strong crystalline rings from titania. According to the STEM-EDS results, vanadium seems to exist preferably on the same locations with titanium in both catalysts (oxygen

**Table 4**
BET-BJH and catalyst composition (calculated from XRF) results of the TiSi supports and 3% vanadia catalysts.

| | Surface area | Pore volume | Pore size | V surface density | XRF | | |
|---|---|---|---|---|---|---|---|
| | [m$^2$ g$^{-1}$] | [cm$^3$ g$^{-1}$] | [nm] | [V nm$^{-2}$] | $V_2O_5$ [%] | $SiO_2$ [%] | $TiO_2$ [%] |
| Ti | 47 | 0.18 | 15 | – | – | – | n.a |
| TiSi(5) | 89 | 0.37 | 16 | – | – | 4.4 | 97.0 |
| 3V/Ti | 59 | 0.20 | 14 | 3.25 | 2.9 | – | 92.8 |
| 3V/TiSi(5) | 84 | 0.32 | 16 | 2.39 | 2.9 | 3.5 | 90.3 |

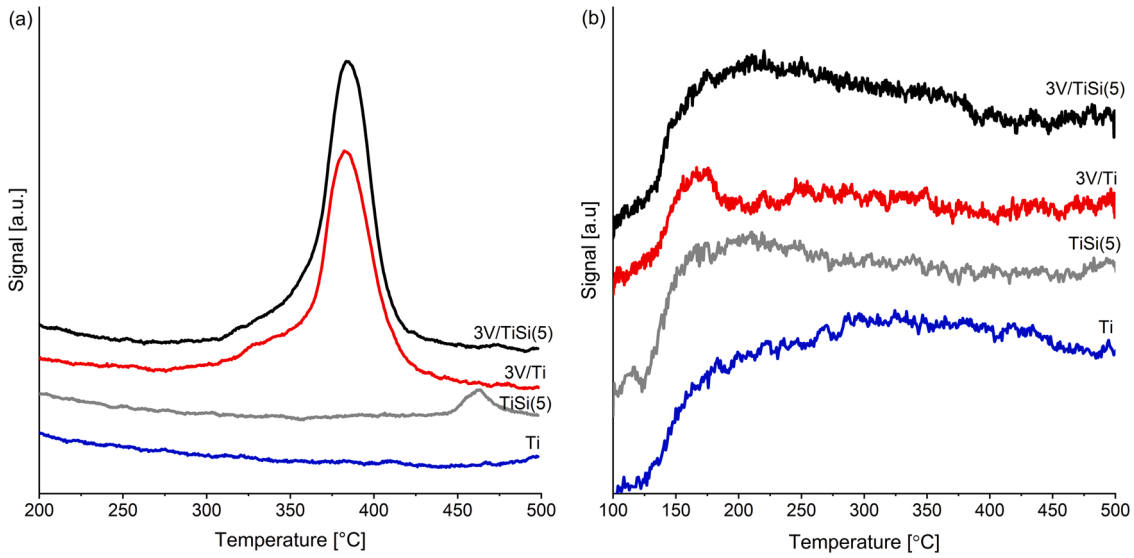


**Fig. 8.** (a) $H_2$-TPR and (b) $NH_3$-TPD profiles of reference catalysts 3V/Ti and 3V/TiSi(5) collected in the temperature range of 100/200–500 °C with the heating rate of 10 °C $min^{-1}$.

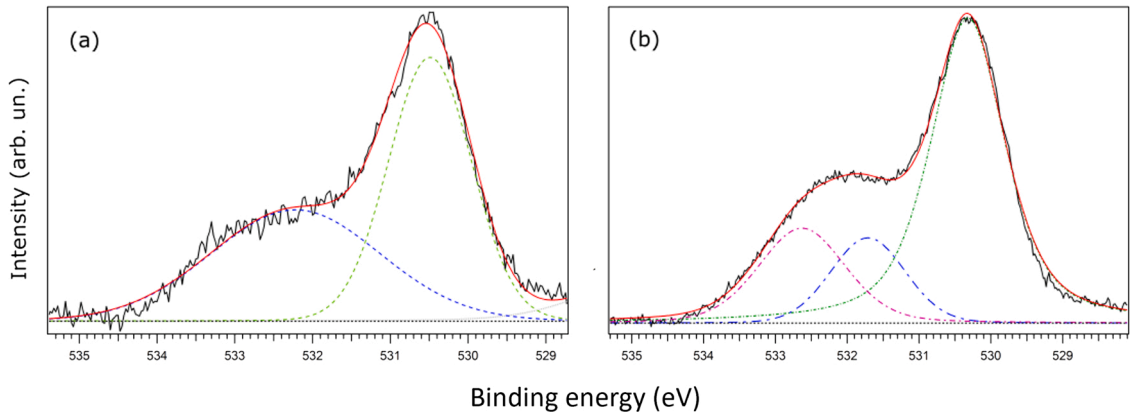


**Fig. 9.** Electron spectra of (a) 3V/Ti and (b) 3V/TiSi(5) covering O1s photoelectron peaks.

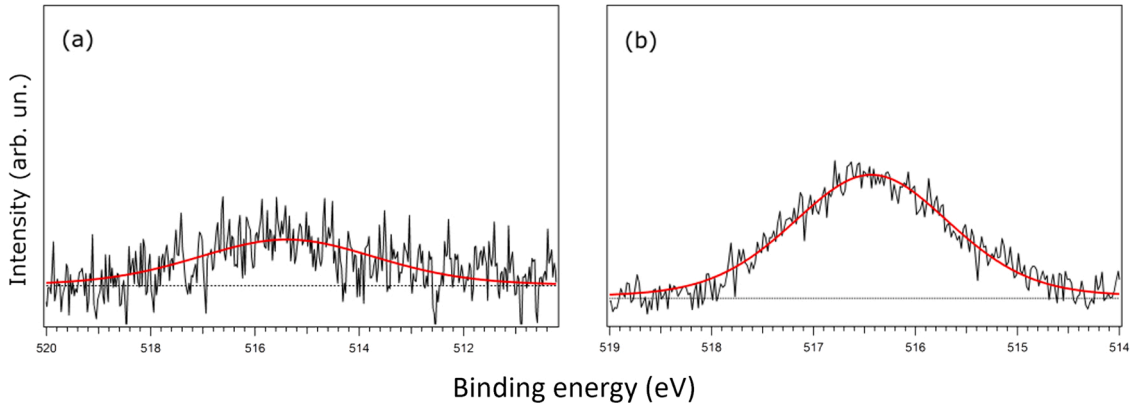


**Fig. 10.** Electron spectra of (a) 3V/Ti and (b) 3V/TiSi(5) covering V2$p_{3/2}$ photoelectron peaks.

is excluded from the images). In the 3V/TiSi(5) sample (Fig. S6b), the amount of silica seems to vary from area to area being even challenging to detect by EDS in some places.

When comparing the sol-gel prepared SiTi(30) catalysts and the reference TiSi(5) catalysts, the TPR results show that the titania-rich materials are reduced more easily. This may partly explain why only the $V^{4+}$ oxidation state is observed for the TiSi(5) and Ti catalysts while for SiTi(30) $V^{5+}$ co-exists. The effect of UHV on the results was shown earlier by Kokkonen et al. [64], and was aimed to be minimized in this study by using APXPS in case of reference catalysts. Hydrogen consumed during the $H_2$-TPR experiment of the reference catalysts (0.0143 mmol) was equal to the theoretical requirement for the reduction of vanadia

from 5+ to 3+ oxidation state (0.0145 mmol) in the catalysts. Thus, it is expected that the support may reduce only slightly between the temperature level of 350–420 °C while most of hydrogen is consumed due to vanadia reduction.

Fig. 11 shows the Raman spectra of the TiSi samples at 100 °C and 400 °C between 100 and 1100 $cm^{-1}$. Raman bands are observed at ~154, 205, 395, 509 and 634 $cm^{-1}$, which can be assigned as the anatase-phase of titania. No clear spectral features related to silica compounds are observed. A Raman band related to the symmetric stretch of the mono-oxo terminal V=O bond appears at ~1030 $cm^{-1}$ [22]. This is the most intense for the vanadia catalyst supported on pure titania. For 3V/TiSi(5), the Raman peak of V=O species is less strong, and an additional peak appears at ~1013 $cm^{-1}$. It has been earlier shown with uv-Raman measurements that V=O stretching mode of surface $VO_x$ species may appear at 1013 $cm^{-1}$ for low surface coverages and shift higher wavenumber when increasing the surface coverage. Based on this observation, the lower wavenumber V=O peak would be related to isolated $VO_x$ species while the higher wavenumber peaks to polymerized $VO_x$ species. [41] The somewhat surprising appearance of 1013 $cm^{-1}$ peak for the 3V/TiSi(5) catalyst could then indicate the presence of both types of $VO_x$ species, while in the case of the Ti-support, only polymerized $VO_x$ species exist. Raman-results thus support the observations of APXPS measurements, where only $V^{4+}$ oxidation state was observed. For the titania-rich reference catalysts, the existence of crystalline anatase is evident, while in the sol-gel prepared materials the result is inconclusive. Furthermore, the spectral features indicating a mixed-oxide phase are not observed in the Raman analysis of the reference catalysts. The vanadia species in the sol-gel prepared samples were slightly different depending on the calcination atmosphere. The air calcined samples contained more isolated $VO_x$ species and less polymeric species than $N_2$ calcined. Furthermore, indications of the possible presence of $V_2O_5$ microcrystals were observed for the stagnant-air calcined samples. Thus, the vanadia species of the air flow calcined sol-gel and the reference 3V/TiSi(5) catalyst are quite similar based on Raman. The vanadia oxidation state is more stable in the case of the sol-gel prepared mixed oxide support than in the case of the reference support having the crystalline anatase structure.

### 3.4. *In-situ oxidative dehydrogenation of methanol over titania-rich catalysts*

The *in situ* DRIFT results for TiSi(5) and 3V/TiSi(5) are presented in Figs. 12 and 13. The wavenumbers of adsorbed methoxy species are presented in Table 5 along with the peak surface areas. The methoxy peaks observed are closer to those reported for single oxides by Burcham et al. [22] compared to the SiTi(30)-supported catalysts. This may be due to the mixed-oxide structure of the sol-gel prepared catalysts and possible separate phases of $TiO_2$ anatase and $SiO_2$ in the reference catalysts. In the case of TiSi(5) support, an increase in temperature leads to a decrease in the intensities of the peaks indicating adsorbed methoxy species. However, it seems that methoxy species is more strongly bound

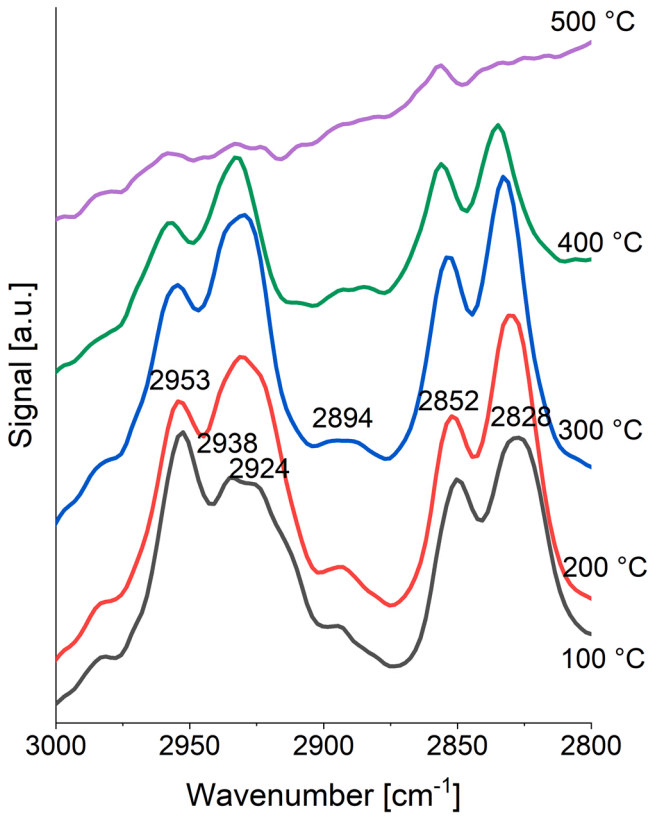


**Fig. 12.** *In situ* DRIFT spectra in the C–H stretching region of the TiSi(5) support under an air flow at temperatures from RT to 500 °C.

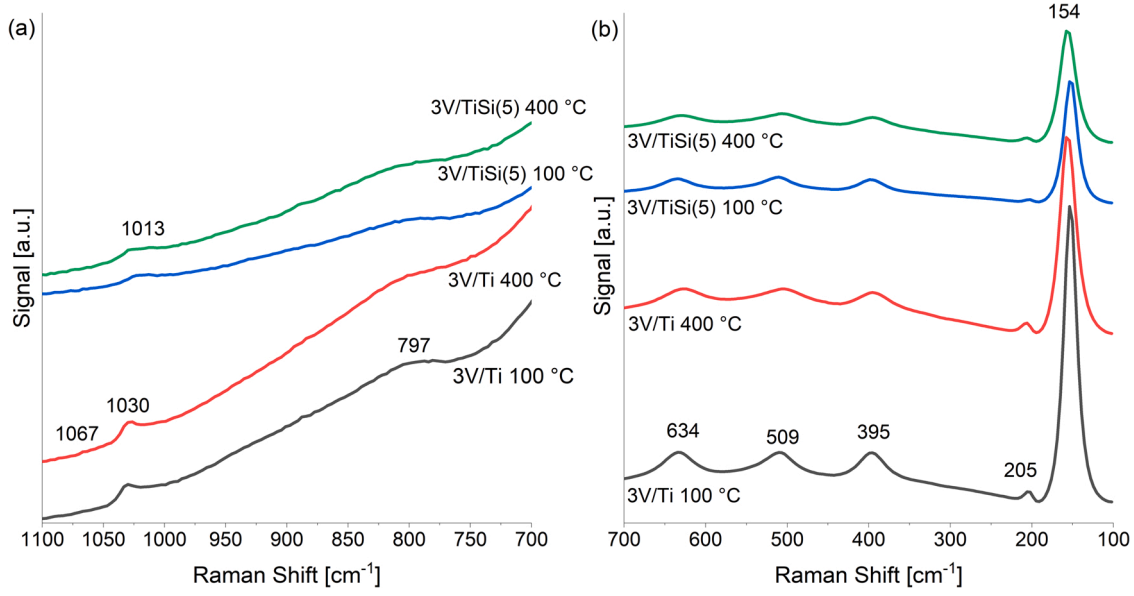


**Fig. 11.** Raman spectra of Ti and TiSi(5) supported vanadia catalysts at 100 °C and 400 °C between (a) 900–1100 $cm^{-1}$ and (b) 100–700 $cm^{-1}$.

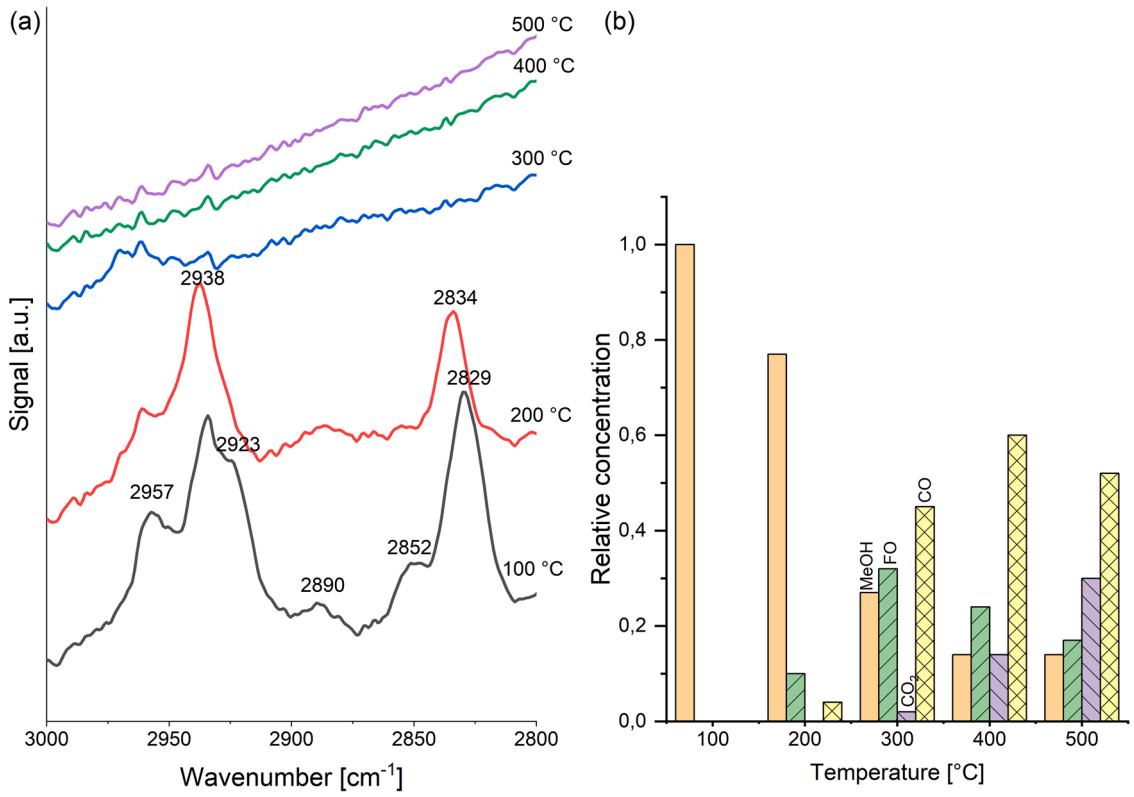


**Fig. 13.** (a) *In situ* DRIFT spectra in the C–H stretching region for the 3 V/TiSi(5) catalyst under an air flow for ~5 min after 2000 ppm methanol (in air) injection into the sample cell at temperatures from 100–500 °C, (b) Relative gas concentrations measured during the experiment.

**Table 5**
Observed peak positions and integrated peak surface areas for the adsorbed methoxy species on the TiSi(5) catalysts during methanol reaction at temperatures from 100 °C to 500 °C.

| Temperature | TiSi (5) | | 3V/TiSi (5) | | | |
|---|---|---|---|---|---|---|
| | Si-$OCH_3$ | Ti-$OCH_3$ | Si-$OCH_3$ | Ti-$OCH_3$ | V-$OCH_3$ | Formaldehyde re-adsoprtion |
| Peak position ($cm^{-1}$) | 2852 2953 | 2828 2924 | 2852 2957 | 2829 2923 | 2834 2938 | 2890 |
| | Peak surface area | | | | | |
| 100 °C | 1.636 | 1.513 | 0.094 | 0.203 | 0.099 | 0.014 |
| 200 °C | 1.653 | 1.905 | 1.725 | 1725 | 2.461 | 1.030 |
| 300 °C | 1.809 | 2.060 | * | * | * | * |
| 400 °C | 1.278 | 1.357 | * | * | * | * |
| 500 °C | * | * | * | * | * | * |

*not detected

on the Si-sites, since it can still be observed at 500 °C. The increase in temperature leads also to a slight shift of the methoxy peaks towards higher wavenumbers. A weak band at 2887–2894 $cm^{-1}$ is assigned to the overlapping mode from the second methoxy overtone band. The symmetric C-H stretch of surface formate species ($HCOO^-$) is visible at ~2894 $cm^{-1}$. It indicates the re-adsorption of the product, *i.e.*, formaldehyde during the MeOH reaction [22].

The decrease in the methoxy peak intensities is more clearly visible in the case of 3V/TiSi(5), where methoxy groups practically disappear already at 300 °C (Fig. 13a). This result demonstrates an increase in the reaction rate in the presence of vanadia. Even for the higher (3%) vanadia loading, the distinction between V-$OCH_3$ and Ti-$OCH_3$ is rather difficult. A similar temperature-induced upward shift is observed for methoxy species adsorbed on the 3V/TiSi(5) catalyst than in the case of the support. The V-$OCH_3$ vibration can be observed at 2938 $cm^{-1}$ (100 °C), where two separate peaks can be distinguished. At 200 °C, V-$OCH_3$ is visible at 2834 and 2938 $cm^{-1}$. Fig. 13b shows methanol and product concentrations measured during the DRIFT studies at different reaction temperatures. Formaldehyde appears already at 200 °C, reaching the maximum at 300 °C and then starting to decrease due to the MeOH complete oxidation and formaldehyde oxidation further to CO and $CO_2$ as presented with Reactions 1–4. Here the re-adsorption of formaldehyde as formate can be observed as the band appears at 2890 $cm^{-1}$ (at 100 °C and 200 °C) similarly to the TiSi(5) support. The measured feed and product concentrations during the *in situ* MeOH studies are presented for the TiSi(5) support in the supplementary material (Fig. S14).

Table 5 shows the calculated methoxy peak areas for the TiSi(5) support and the 3V/TiSi(5) catalyst. For 3V/TiSi(5), the values for V-$OCH_3$ and formaldehyde re-adsorption are shown. The surface areas of the peaks increase when rising the temperature. Fig. S12 in the supplementary material shows the deconvolution of the methoxy peaks for the reference materials at 100 °C and 200 °C. In the case of the 3V/TiSi (5) catalyst, formaldehyde concentration reaches maximum at 300 °C. The temperature where only Si-$OCH_3$ species are visible in the FTIR spectrum is reached at 300 °C (amount not quantified due to low intensity). This is similar with the results observed for the 1.5V/TiSi(30) catalyst, since the highest formaldehyde production was observed after the amount of surface methoxy species started to decrease. In the case of the SiTi(30)-catalysts, the Ti-$OCH_3$ species were stable up to 400 °C, while in the case of TiSi(5), the Ti-$OCH_3$ species were not anymore observed at 300 °C. It seems that the stability of the methoxy species on the support has a connection to formaldehyde production. The more stable the species at higher temperature, the higher amount of formaldehyde is produced. The 1.5V/SiTi(30) catalyst is able to produce higher amounts of formaldehyde at higher temperature, while the 3V/TiSi(5) catalyst is active at lower temperature, but a lower amount of formaldehyde is formed, and reaction proceeds towards complete oxidation at lower temperature range. Re-adsorption of formaldehyde is observed for the 3V/TiSi(5) catalyst already at 100 °C until 200 °C after which CO

and $CO_2$ starts to form. Re-adsorption of formaldehyde seems to be an indication for its further oxidation.

### 3.5. Catalyst activity studies

#### 3.5.1. Methanol oxidative dehydrogenation to formaldehyde

To complete the study of the vanadia catalysts, the comparison of the activities of the sol-gel prepared 1.5V/SiTi(30) catalysts with the reference catalysts in methanol oxidative dehydrogenation were performed in a fixed bed tubular reactor. The formation of formaldehyde and consumption of MeOH during the oxidation of 1000 ppm methanol are presented in Fig. 14. The performance of the catalysts follows the observations of the *in situ* DRIFT studies. Formaldehyde formation temperature is 250 °C lower over the 3V/TiSi(5) reference catalyst compared to the sol-gel prepared SiTi(30) supported catalysts. However, all the sol-gel prepared catalysts with a lower vanadia amount result in higher formaldehyde concentration. With 3V/TiSi(5), the oxidation towards CO occurs simultaneously with a rapid decrease in the formaldehyde concentration at rather low temperature. The $CO_2$ formation (not shown in the figure) remains below 100 ppm in all the cases reaching the highest value with the 3V/TiSi(5) catalyst. These results are qualitatively consistent with the observations of the *in situ* DRIFT studies.

In connection with the methanol DRIFT-studies we concluded that the silicon sites retain methoxy-groups at higher temperature than the titanium sites, which could explain the differences in the temperatures observed for the formaldehyde formation. The TiSi(5) catalysts are reduced more easily. Easier reducibility has evidently a connection with the low temperature formaldehyde formation observed for the TiSi(5) catalyst, but also further oxidation of formaldehyde observed at around 250 °C. Easier reducibility of the catalyst is also beneficial for the Mars van Krevelen type of a reaction mechanism. The 1.5V/SiTi(30) catalysts are also more acidic compared to the 3V/TiSi(5) catalyst, which has been shown earlier to be related to high selectivity towards formaldehyde production [82]. The 1.5V/SiTi(30) catalysts seem also to have a higher relative amount of polymeric $VO_x$ species compared to monomeric $VO_x$. These aspects may explain the higher formaldehyde production observed for all the 1.5V/SiTi(30) catalysts.

#### 3.5.2. Formaldehyde production from the contaminated methanol

One of the goals of the current work was to study the catalytic materials in the presence of sulfur contaminant. First, the activities of the supports, *i.e.*, SiTi(30) and TiSi(5), in the conversion of methanol and methyl mercaptan to formaldehyde are presented in Fig. 15. At 500 °C, the formaldehyde formation in the case of TiSi(5) is higher than with SiTi(30). The reference TiSi(5) reaches the highest formaldehyde concentration at 380 °C. For the SiTi(30) catalyst, the temperature needs to be 535 °C to reach approximately the same formaldehyde concentration. This result is consistent with the earlier findings and suggests also that the maximum formaldehyde concentration is not reached at the maximum temperature of the experiment.

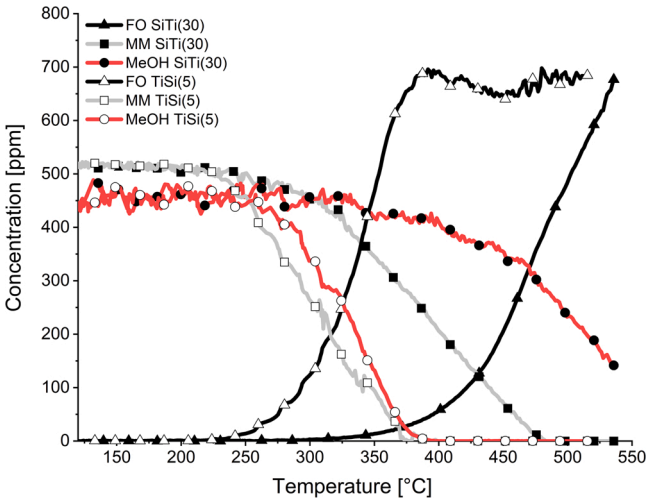


**Fig. 15.** Formation of formaldehyde in the oxidation of a mixture of 500 ppm methanol and 500 ppm methyl mercaptan from 100 °C to ~500 °C with the support materials of SiTi(30) and TiSi(5) (supports ground to a similar particle size).

The addition of vanadium into the SiTi(30) support improved the performance of the catalyst only slightly (See comparison in supplementary Fig. S15), while we have earlier observed a clear positive impact after addition of vanadia [14]. Differences between the results can be explained by the quality of vanadia species demonstrating their importance. The differences between the catalysts calcined at different atmospheres were not significant in the case of simultaneous reaction of methanol and methyl mercaptan. (See supplementary Fig. S16).

The results of the oxidation experiments for 1.5V/SiTi(30)$_{AF}$ are presented in Fig. 16. The maximum formaldehyde formation was not reached at maximum temperature of experiment, and at 500 °C it was only 60 ppm higher than in the case of the corresponding support. $SO_2$ was formed according to the main methyl mercaptan (MM) oxidation reaction to formaldehyde. The formation of DMDS was observed above

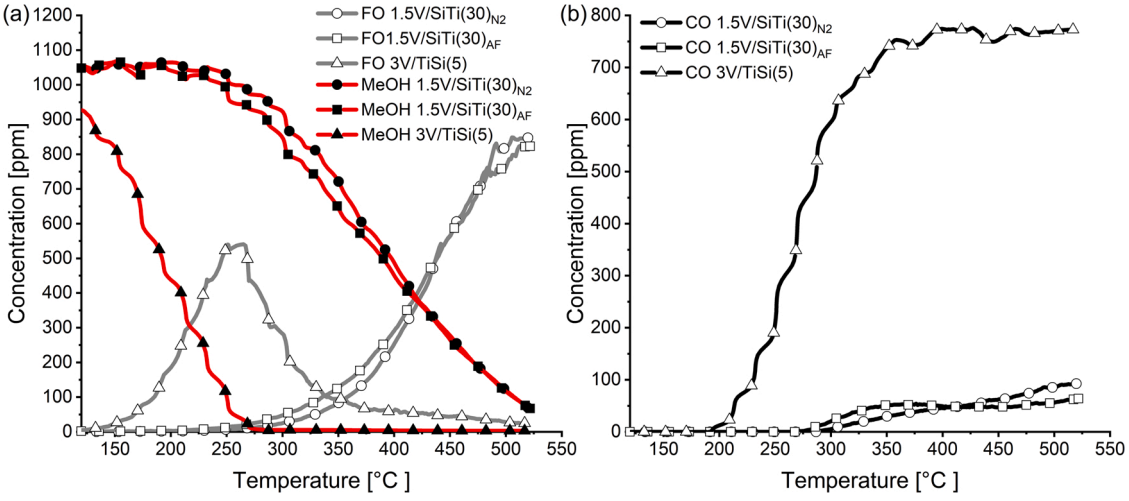


**Fig. 14.** Oxidation of 1000 ppm methanol over the air and $N_2$ calcined 1.5V/SiTi(30) and 3V/TiSi(5) catalysts. (a) Formation of formaldehyde (FO), (b) Formation of carbon monoxide (CO) in the temperature range of 120–500 °C.

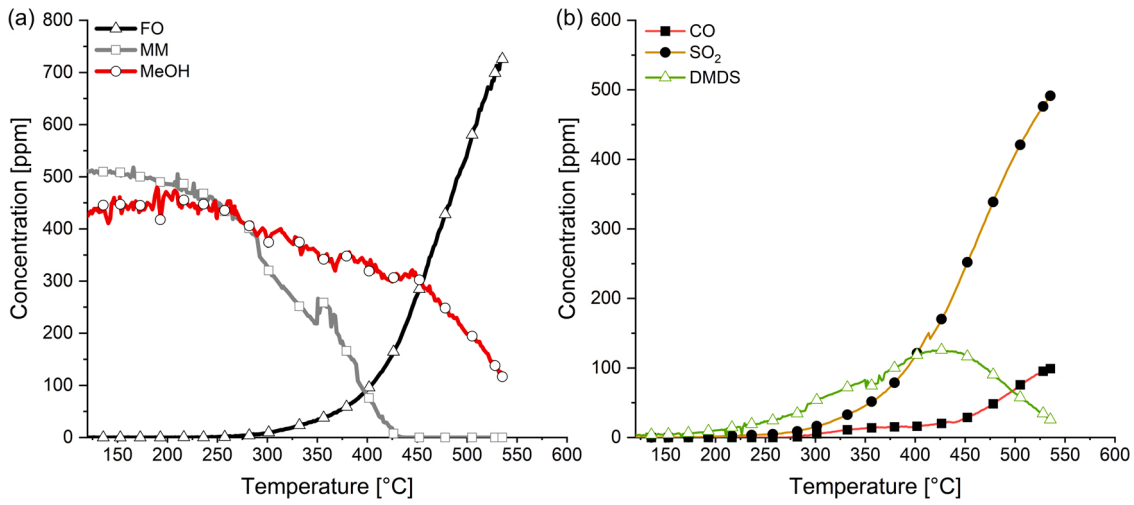


**Fig. 16.** Simultaneous conversion of 500 ppm methanol and 500 ppm methyl mercaptan to formaldehyde in the temperature range of 100–500 °C with 1.5%V/SiTi (30) calcined in flowing air (a) Concentration of MeOH, MM and FO (b) Concentration of by-products CO, $SO_2$ and DMDS.

200 °C reaching the highest concentration of ~115 ppm at 430 °C.

The performance of the 3V/TiSi(5) reference catalyst (powder form) was also studied in the oxidation of a mixture of methyl mercaptan and methanol. The results are shown in Fig. 17. The formation of formaldehyde takes place at temperatures that are over 200 °C lower than in the case of 1.5V/SiTi(30)$_{AF}$ catalysts presented in Fig. 16. The maximum formaldehyde formation was reached at 310 °C, while the maximum was not reached with 1.5V/SiTi(30)$_{AF}$ at the maximum temperature of the experiment. The $SO_2$ formation in the case of both catalysts was at similar level, however, the CO formation in the case of the 3V/TiSi(5) catalyst was significantly higher indicating further oxidation of organic species. This is consistent with the *in situ* experiments. Furthermore, the $CO_2$ formation is observed already at around 450 °C.

Methyl mercaptan is oxidized more easily compared to methanol, which has been earlier reported by Koivikko et al. [13], and it typically shifts the methanol conversion towards slightly higher temperatures in the case of oxidation of the mixture. This was observed in the cases of 1.5V/SiTi(30)$_{AF}$ and 3V/TiSi(5) reference catalyst. Temperature shift was also visible in the formaldehyde formation over the 3V/TiSi(5) reference catalyst, where optimum formaldehyde formation temperature increased by about 50 °C. It was not possible to observe the same change in the case of 1.5V/SiTi(30)$_{AF}$ due to the used temperature range.

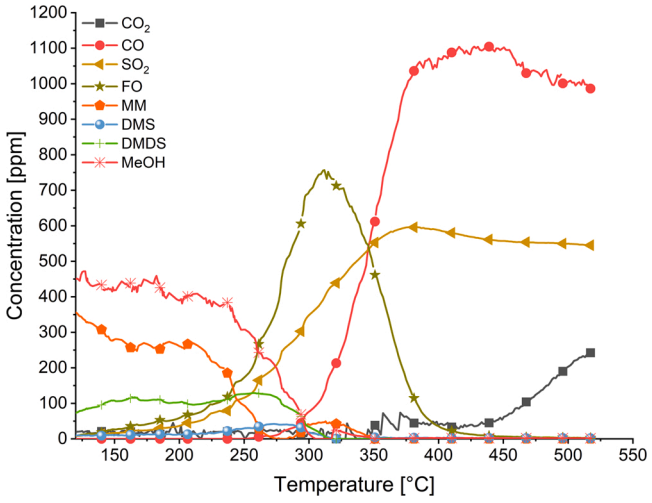


**Fig. 17.** Simultaneous conversion of 500 ppm methanol and 500 ppm methyl mercaptan to formaldehyde over the 3V/TiSi(5) reference catalyst in the temperature range of 100–500 °C.

The reference catalysts 3V/TiSi(5) and 3V/Ti were also available in monolith forms, and their activities were evaluated in the reaction of the mixture of methanol and methyl mercaptan (Fig. 18). It was observed that the conversion of MM over both the monolith-form reference catalysts started already below 200 °C (appearance of DMDS and DMS) and signs of further oxidation were notable already above 300 °C by the appearance of CO and $CO_2$ as the reaction products. The catalysts reach optimal formaldehyde formation at 350 °C, which is a bit higher than in the case of the powder-form catalyst. However, the maximum FO concentration reached is only ~550 ppm, which is notably less than that of the powder-form catalyst. The reaction towards complete oxidation products occurs above 350 °C. From the results, it is also visible that the silica containing catalyst can keep the formaldehyde formation at a higher level at higher temperatures. The result is in accordance with the earlier observations related to silica, that adsorbs methoxy species at higher temperature. The catalyst supported only on titania shows higher formation of CO and $CO_2$ than the one supported on titania-silica, and the effect is visible with a low silica content, *i.e.*, only 5%. This effect seems mainly to be related to the support properties that also affect the quality of vanadium species.

## 4. Conclusions

The $V_2O_5$ catalysts supported on $SiO_2$-$TiO_2$ were prepared, characterized and applied in oxidative dehydrogenation of methanol aiming at utilization of the emissions of volatile organic compounds. The reaction was studied using *in situ* DRIFT and light-off experiments. The activities of the materials were evaluated also in presence of methyl mercaptan, which was used to simulate the utilization of contaminated methanol in chemicals production.

The catalytic materials were a self-made silica-rich mixed oxide (Si/Ti 70/30) catalyst containing 1.5% vanadia and a reference catalyst having 3% vanadia supported on Ti/Si (95/5) or anatase $TiO_2$. The self-made sol-gel catalysts were calcined in different gas conditions. The following main conclusions can be drawn:

- The sol-gel prepared catalysts were amorphous, and the mixed oxide structure was evidenced by Time-gated Raman spectroscopy and XPS. The reference catalysts were mainly composed of crystalline anatase. This reflects to higher specific surface area of the sol-gel made catalysts and their lower surface $VO_x$ density.
- Different calcination atmospheres led to formation of different surface vanadia species. All the sol-gel catalysts contained polymeric

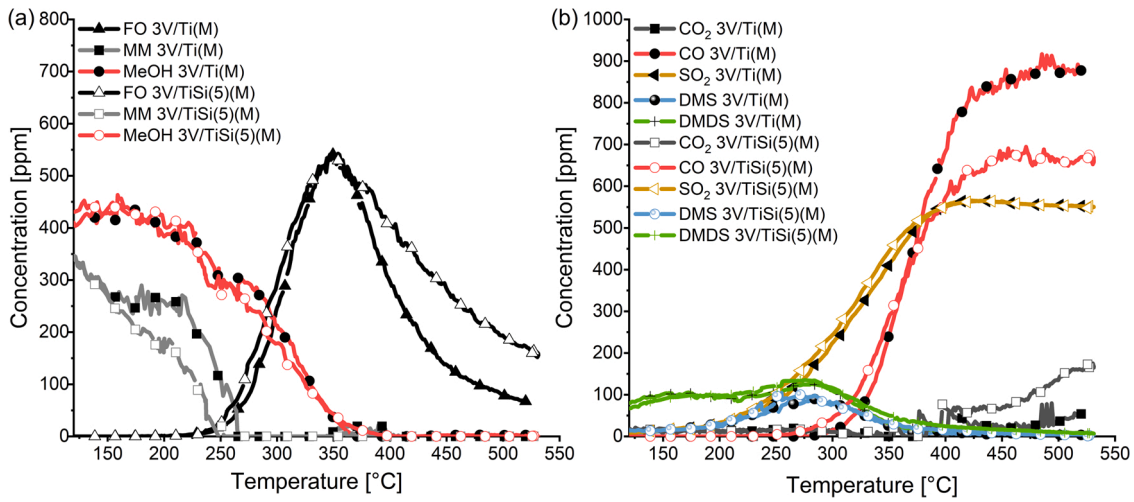


**Fig. 18.** Oxidation of 500 ppm methanol and 500 ppm methyl mercaptan to formaldehyde in the temperature range of 100–500 °C with the 3%V monolith (M) catalysts. (a) Concentration of MeOH, MM and FO, (b) Formation of by-products $CO_2$, CO, $SO_2$, DMS and DMDS.

vanadia species, which amount was highest for the $N_2$ calcined catalyst. The stagnant air calcined catalyst contained also $V_2O_5$. Heating of the catalyst during *in situ* Raman analysis revealed changes in the composition of vanadia species. The amount of $V_2O_5$ on the stagnant air catalyst decreased, and quantity of other species increased. Polymeric species reached the maximum at 500 °C in case of $N_2$ and stagnant air calcined catalyst. For the catalyst calcined under air flow, the maximum appeared at 300 °C.

- The $TiO_2$-supported reference catalyst had only polymeric $VO_4$ species, while the addition of 5% silica in the support modified the vanadia species leading to coexistence of isolated $VO_x$ species.
- Vanadia species exist preferably on titania surface.
- The vanadium oxidation state was more stable when it was supported on the sol-gel prepared amorphous mixed oxide catalyst, which was shown by difficult reduction and possibility to observe also the $V^{5+}$ states in (UHV)XPS. Clear reduction of vanadia was observed between 350 and 420 °C in the case of the reference catalysts containing anatase.
- The acidity of the sol-gel prepared catalysts was significantly higher than that of the reference catalysts. The acidity of the catalyst has a significant role in adsorption of methanol as the first reaction step.
- Good reducibility at lower temperature results in the formation of formaldehyde at lower temperature but leads also to further oxidation of formaldehyde at lower temperature levels. Further oxidation of formaldehyde requires a re-adsorption step.
- Different calcination environments (air stagnant, air flow and $N_2$ flow) did not alter the performance of the catalyst in oxidative dehydrogenation of methanol in the presence of methyl mercaptan, although differences were observed during *in situ* experiments and characterization. During *in situ* DRIFT experiments, the $N_2$ calcined catalyst produced higher amount of formaldehyde than air flow calcined catalyst, that reached the highest formaldehyde production at same temperature range. This might be due to the stability of polymeric vanadia species on the $N_2$ calcined catalyst at higher temperature.

## CRediT authorship contribution statement

**Niina Koivikko:** Methodology, Investigation, Formal analysis, Writing – original draft, Funding acquisition. **Satu Ojala:** Supervision, Conceptualization, Funding acquisition, Investigation, Writing – original draft, Writing – review & editing. **Tiina Laitinen:** Investigation, Visualization, Writing – review & editing. **Felipe Lopes da Silva:** Investigation, Visualization. **Lauri Hautala:** Formal analysis, Visualization. **Zouhair El Assal:** Investigation – review & editing. **Mari Honkanen:** Investigation, Resources, Formal analysis, Data curation, Visualization, Writing – review & editing. **Minnamari Vippola:** Resources, Data curation, Writing – review & editing. **Mika Huuhtanen:** Investigation, Writing – review & editing, **Marko Huttula:** Writing – review & editing. **Teuvo Maunula:** Resources, Writing – review & editing. **Riitta L. Keiski:** Supervision, Conceptualization, Funding acquisition, Writing – original draft, Writing – review & editing.

## Declaration of Competing Interest

The authors declare that they have no known competing financial interests or personal relationships that could have appeared to influence the work reported in this paper.

## Data Availability

The data is not available at the moment; some data may later be available on request.

## Acknowledgements

This work was carried out with the financial support of the Academy of Finland (ELECTRA-project, grant numbers 289266, 294063 and 319448), the Finnish foundation of technology promotion, Jenny and Antti Wihuri foundation and Jorma and Riitta Takanen foundation. Otto A. Malm foundation and Tauno Tönning Foundation are also acknowledged. Kaisu Ainassaari and Markus Riihimäki are acknowledged for their valuable help with the characterization of catalysts. Part of the work was carried out with the support of the Centre for Material Analysis, University of Oulu, Finland. Analytical (S)TEM work made use of Tampere Microscopy Center facilities at Tampere University, Finland.

## Appendix A. Supporting information

Supplementary data associated with this article can be found in the online version at doi:10.1016/j.apcatb.2022.121803.

## References

[1] G. Reuss, W. Disteldorf, A.O. Gamer, A. Hilt, Formaldehyde, Ulmann's Encycl. IIndustrial Chem. 15, 2012, 735–768. https://doi.org/10.1002/14356007.a11.
[2] C. Chen, Y. Cao, S. Liu, J. Chen, W. Jia, Review on the latest developments in modified vanadium-titanium-based SCR catalysts, Cuihua Xuebao Chin. J. Catal. 39 (2018) 1347–1365, https://doi.org/10.1016/S1872-2067(18)63090-6.

[3] S. Pitkäaho, S. Ojala, T. Maunula, A. Savimäki, T. Kinnunen, R.L. Keiski, Oxidation of dichloromethane and perchloroethylene as single compounds and in mixtures, Appl. Catal. B Environ. 102 (2011) 395–403, https://doi.org/10.1016/j.apcatb.2010.12.011.

[4] G. Deo, I.E. Wachs, Reactivity of Supported Vanadium Oxide Catalysts: The Partial Oxidation of Methanol, 334, 1994, 323–334.

[5] G. Deo, I.E. Wachs, Effect of Additives on the Structure and Reactivity of the Surface Vanadium Oxide Phase in V2O5/TiO2 Catalysts, 345, 1994, 335–345.

[6] Q. Sun, J.M. Jehng, H. Hu, R.G. Herman, I.E. Wachs, K. Klier, In situ Raman spectroscopy during the partial oxidation of methane to formaldehyde over supported vanadium oxide catalysts, J. Catal. 165 (1997) 91–101, https://doi.org/10.1006/jcat.1997.1446.

[7] T. Kim, I.E. Wachs, CH 3 OH oxidation over well-defined supported V2O5/Al2O3 catalysts: Influence of vanadium oxide loading and surface vanadium – oxygen functionalities, 255 (2008) 197–205. https://doi.org/10.1016/j.jcat.2008.02.007.

[8] J.M. Jehng, G. Deo, B.M. Weckhuysen, I.E. Wachs, Effect of water vapor on the molecular structures of supported vanadium oxide catalysts at elevated temperatures, J. Mol. Catal. A Chem. 110 (1996) 41–54, https://doi.org/10.1016/1381-1169(96)00061-1.

[9] R.Z. Khaliullin, A.T. Bell, A density functional theory study of the oxidation of methanol to formaldehyde over vanadia supported on silica, titania, and zirconia, J. Phys. Chem. B 106 (2002) 7832–7838, https://doi.org/10.1021/jp014695h.

[10] I.E. Wachs, Catalysis science of supported vanadium oxide catalysts, Dalton Trans. 42 (2013) 11762, https://doi.org/10.1039/c3dt50692d.

[11] B.M. Weckhuysen, D.E. Keller, Chemistry, spectroscopy and the role of supported vanadium oxides in heterogeneous catalysis, Catal. Today 78 (2003) 25–46, https://doi.org/10.1016/S0920-5861(02)00323-1.

[12] W.C. Vining, A. Goodrow, J. Strunk, A.T. Bell, An experimental and theoretical investigation of the structure and reactivity of bilayered VOx/TiOx/$SiO_2$ catalysts for methanol oxidation, J. Catal. 270 (2010) 163–171, https://doi.org/10.1016/j.jcat.2009.12.017.

[13] N. Koivikko, T. Laitinen, S. Ojala, S. Pitkäaho, A. Kucherov, R.L. Keiski, Formaldehyde production from methanol and methyl mercaptan over titania and vanadia based catalysts, Appl. Catal. B Environ. 103 (2011) 72–78, https://doi.org/10.1016/j.apcatb.2011.01.010.

[14] N. Koivikko, T. Laitinen, A. Mouammine, S. Ojala, R.L. Keiski, Catalytic Activity Studies of Vanadia / Silica – Titania Catalysts in SVOC Partial Oxidation to Formaldehyde: Focus on the Catalyst Composition, 2018. https://doi.org/10.3390/catal8020056.

[15] T. Laitinen, S. Ojala, R. Cousin, N. Koivikko, C. Poupin, Z. El Assal, A. Aho, R. L. Keiski, Activity, selectivity, and stability of vanadium catalysts in formaldehyde production from emissionsof volatile organic compounds, J. Ind. Eng. Chem. 83 (2020) 375–386, https://doi.org/10.1016/j.jiec.2019.12.011.

[16] E. Tella, A. Trimpalis, A. Tsevis, C. Kordulis, A. Lycourghiotis, S. Boghosian, K. Bourikas, Advanced synthesis and characterization of vanadia/titania catalysts through a molecular approach, Catalysts 11 (2021) 1–21, https://doi.org/10.3390/catal11030322.

[17] H. Wang, Q. Liu, C. You, Regeneration of sulfur-deactivated $TiO_2$ photocatalysts, Appl. Catal. A Gen. 572 (2019) 15–23, https://doi.org/10.1016/j.apcata.2018.12.031.

[18] B.M. Reddy, I. Ganesh, E.P. Reddy, Study of dispersion and thermal stability of $V_2O_5/TiO_2$ –$SiO_2$ catalysts by XPS and other techniques, J. Phys. Chem. B. 101 (1997) 1769–1774, https://doi.org/10.1021/jp963091o.

[19] X. Gao, S.R. Bare, J.L.G. Fierro, I.E. Wachs, Structural characteristics and reactivity/reducibility properties of dispersed and bilayered $V_2O_5/TiO_2/SiO_2$ catalysts, J. Phys. Chem. B 103 (1999) 618–629, https://doi.org/10.1021/jp983357m.

[20] S. Bagheri, N. Muhd Julkapli, S. Bee Abd Hamid, Titanium dioxide as a catalyst support in heterogeneous catalysis, Sci. World J. 2014 (2014), https://doi.org/10.1155/2014/727496.

[21] B. Darif, Synthesis and characterization of catalysts used for the catalytic oxidation of sulfur-containing volatile organic compounds: focus on sulfur-induced deactivation, 2016.

[22] L.J. Burcham, G. Deo, X. Gao, I.E. Wachs, In situ IR, Raman, and UV-Vis DRS spectroscopy of supported vanadium oxide catalysts during methanol oxidation, Top. Catal. 11–12 (2000) 85–100, https://doi.org/10.1023/A:1027275225668.

[23] X. Gao, S.R. Bare, J.L.G. Fierro, M.A. Banares, I.E. Wachs, Preparation and in-situ spectroscopic characterization of molecularly dispersed titanium oxide on silica, J. Phys. Chem. B 102 (1998) 5653–5666, https://doi.org/10.1021/jp981423e.

[24] S. Ojala, N. Koivikko, T. Laitinen, A. Mouammine, P. Seelam, S. Laassiri, K. Ainassaari, R. Brahmi, R. Keiski, Utilization of utilization of volatile organic compounds as an alternative for destructive abatement, Catalysts 5 (2015) 1092–1151, https://doi.org/10.3390/catal5031092.

[25] A. Mouammine, S. Ojala, L. Pirault-Roy, M. Bensitel, R. Keiski, R. Brahmi, Catalytic partial oxidation of methanol and methyl mercaptan: Studies on the selectivity of $TiO_2$ and $CeO_2$ supported $V_2O_5$ catalysts, Top. Catal. 56 (2013) 650–657, https://doi.org/10.1007/s11244-013-0024-3.

[26] L.J. Burcham, L.E. Briand, I.E. Wachs, Quantification of active sites for the determination of methanol oxidation turn-over frequencies using methanol chemisorption and in situ infrared techniques. 2 - Bulk metal oxide catalysts, Langmuir 17 (2001) 6175–6184, https://doi.org/10.1021/la010010t.

[27] Q. Wang, R.J. Madix, Partial oxidation of methanol to formaldehyde on a model supported monolayer vanadia catalyst: Vanadia on $TiO_2$(1 1 0), Surf. Sci. 496 (2002) 51–63, https://doi.org/10.1016/S0039-6028(01)01600-4.

[28] A. Goodrow, A.T. Bell, A theoretical investigation of the selective oxidation of methanol to formaldehyde on isolated vanadate species supported on titania, J. Phys. Chem. C 112 (2008) 13204–13214, https://doi.org/10.1021/jp801339q.

[29] J.L. Bronkema, A.T. Bell, Mechanistic studies of methanol oxidation to formaldehyde on isolated vanadate sites supported on MCM-48 mechanistic studies of methanol oxidation to formaldehyde on isolated vanadate sites supported on MCM-48, J. Phys. Chem. (2007) 14530–14540, https://doi.org/10.1021/jp0653149.

[30] J.L. Bronkema, A.T. Bell, Mechanistic studies of methanol oxidation to formaldehyde on isolated vanadate sites supported on high surface area zirconia, J. Phys. Chem. C 112 (2008) 6404–6412, https://doi.org/10.1021/jp7110692.

[31] W.C. Vining, J. Strunk, A.T. Bell, Investigation of the structure and activity of VOx/ ZrO2/SiO2 catalysts for methanol oxidation to formaldehyde, 281, 2011, 222–230. https://doi.org/10.1016/j.jcat.2011.05.001.

[32] E. Wachs, Production of formaldehyde from methyl mercaptans, 5969191, 1999.

[33] I.E. Wachs, Production of formaldehyde from methyl mercaptans, 5969191, 1999.

[34] R.A. Ross, S.P. Sood, Catalytic oxidation of methyl mercaptan over cobalt molybdate, Ind. Eng. Chem. Prod. Res. Dev. 16 (1977) 147–150, https://doi.org/10.1021/i360062a007.

[35] C.M. Cellier, V. Vromman, V. Ruaux, E.M. Gaigneaux, P. Grange, Sulfation mechanism and catalytic behavior of manganese oxide in the oxidation of methanethiol, J. Phys. Chem. B 108 (2004) 9989–10001, https://doi.org/10.1021/jp049158m.

[36] C. Lahousse, A. Bernier, P. Grange, B. Delmon, P. Papaefthimiou, T. Ioannides, X. Verykios, Evaluation of γ-$MnO_2$ as a VOC removal catalyst: Comparison with a noble metal catalyst, J. Catal. 178 (1998) 214–225, https://doi.org/10.1006/jcat.1998.2148.

[37] A.K. Dalai, E.L. Tollefson, A. Yang, E. Sasaoka, Oxidation of methyl mercaptan over an activated carbon in a fixed-bed reactor, Ind. Eng. Chem. Res. 36 (1997) 4726–4733, https://doi.org/10.1021/ie9701231.

[38] X. Zhang, B. Gao, A. Elise, C. Cao, Y. Li, Adsorption of VOCs onto engineered carbon materials: a review, J. Hazard. Mater. 338 (2017) 102–123, https://doi.org/10.1016/j.jhazmat.2017.05.013.

[39] P. Munnik, M. Wolters, A. Gabrielsson, S.D. Pollington, G. Headdock, J.H. Bitter, P.E. De Jongh, K.P.De Jong, Copper Nitrate Redispersion To Arrive at Highly Active Silica-Supported Copper Catalysts, 2011, 14698–14706. https://doi.org/10.1021/jp111778g.

[40] G. Prieto, J. Zečević, Towards stable catalysts by controlling collective properties of supported metal nanoparticles, 12 (2013). https://doi.org/10.1038/nmat3471.

[41] Z. Wu, H.S. Kim, S. Rugmini, S.D. Jackson, P.C. Stair, Surface structures of vanadium oxide supported on aluminas characterized by ultraviolet and visible raman spectroscopy, ACS Div. Fuel Chem. Prepr. 50 (2005) 181–182.

[42] John R. Rumble, CRC Handbook of Chemistry and Physics, 98th Edition (Internet Version 2018), 98th ed., Boca Raton, FL, n.d.

[43] J.A. Moulijn, A.E. Van Diepen, F. Kapteijn, Catalyst deactivation: Is it predictable? What to do? Appl. Catal. A Gen. 212 (2001) 3–16, https://doi.org/10.1016/S0926-860X(00)00842-5.

[44] Y. Dai, P. Lu, Z. Cao, C.T. Campbell, Y. Xia, The physical chemistry and materials science behind sinter-resistant catalysts, Chem. Soc. Rev. 47 (2018) 4314–4331, https://doi.org/10.1039/c7cs00650k.

[45] T.L. Burgess, A.G. Gibson, S.J. Furstein, I.E. Wachs, Converting waste gases from pulp mills into value-added chemicals, Environ. Prog. 21 (2002) 137–141, https://doi.org/10.1002/ep.670210311.

[46] J.C.M. Bordado, J.F.P. Gomes, Atmospheric emissions of Kraft pulp mills, Chem. Eng. Process. 41 (2002) 667–671, https://doi.org/10.1016/S0255-2701(01)00184-2.

[47] J.R.A. Sietsma, J.D. Meeldijk, J.P. Den Breejen, M. Versluijs-helder, A.J. Van Dillen, P.E. De Jongh, K.P.De Jong, The preparation of supported NiO and $Co_3O_4$ nanoparticles by the nitric oxide controlled thermal decomposition of nitrates 3 (2007) 4547–4549, https://doi.org/10.1002/anie.200700608.

[48] T.M. Eggenhuisen, J.P. Den Breejen, D. Verdoes, P.E. De Jongh, K.P. De Jong, Fundamentals of Melt Infiltration for the Preparation of Supported Metal Catalysts. The Case of Co/SiO2 for Fischer - Tropsch Synthesis, 2010, 18318–18325. https://doi.org/10.1016/j.cattod.2010.02.052.(41).

[49] M. Wolters, L.J.W. Van Grotel, T.M. Eggenhuisen, J.R.A. Sietsma, K.P. De Jong, P. E.De Jongh, Combining confinement and NO calcination to arrive at highly dispersed supported nickel and cobalt oxide catalysts with a tunable particle size, Catal. Today 163 (2011) 27–32, https://doi.org/10.1016/j.cattod.2010.02.052.

[50] S. Zhu, M. Scardamaglia, J. Kundsen, R. Sankari, H. Tarawneh, R. Temperton, L. Pickworth, F. Cavalca, C. Wang, H. Tissot, J. Weissenrieder, B. Hagman, J. Gustafson, S. Kaya, F. Lindgren, I. Kallquist, J. Maibach, M. Hahlin, V. Boix, T. Gallo, F. Rehman, G. D'Acunto, J. Schnadta, A. Shavorskiy, HIPPIE: a new platform for ambient-pressure X-ray photoelectron spectroscopy at the MAX IV Laboratory, J. Synchrotron Radiat. 28 (2021) 624–636, https://doi.org/10.1107/S160057752100103X.

[51] Z. El Assal, S. Ojala, S. Pitkäaho, L. Pirault-Roy, B. Darif, J.D. Comparot, M. Bensitel, R.L. Keiski, R. Brahmi, Comparative study on the support properties in the total oxidation of dichloromethane over Pt catalysts, Chem. Eng. J. 313 (2017) 1010–1022, https://doi.org/10.1016/j.cej.2016.10.139.

[52] I.E. Wachs, Raman and IR studies of surface metal oxide species on oxide supports: Supported metal oxide catalysts, Catal. Today 27 (1996) 437–455, https://doi.org/10.1016/0920-5861(95)00203-0.

[53] X. Gao, S.R. Bare, B.M. Weckhuysen, I.E. Wachs, In situ spectroscopic investigation of molecular structures of highly dispersed vanadium oxide on silica under various conditions, J. Phys. Chem. B 102 (1998) 10842–10852, https://doi.org/10.1021/jp9826367.

[54] G. Liu, Y. Liu, G. Yang, S. Li, Y. Zu, W. Zhang, M. Jia, Preparation of titania-silica mixed oxides by a sol-gel route in the presence of citric acid, J. Phys. Chem. C 113 (2009) 9345–9351, https://doi.org/10.1021/jp900577c.
[55] M.F. Wei Zhang, G.R. Giada Innocenti, N.R.S. Enrique, V. Ramos-Fernandez, Antonio Sepulveda-Escribano, Haihong Wu, Fabrizio Cavani, Understanding the oxidative dehydrogenation of ethyl lactate to ethyl pyruvate over vanadia/titania†, Catal. Sci. Technol. 8 (2018) 3707–3978, https://doi.org/DOI https://doi.org/10.1039/C7CY02309J.
[56] A.R. Puigdollers, P. Schlexer, S. Tosoni, G. Pacchioni, Increasing oxide reducibility: the role of metal/oxide interfaces in the formation of oxygen vacancies, ACS Catal. 7 (2017) 6493–6513, https://doi.org/10.1021/acscatal.7b01913.
[57] R.D. Waclaw Makowski, Joanna Lojewska, TPR and TPD studies of vanadia/silica catalysts for selective oxidation of methane to formaldehyde, React. Kinet. Catal. Lett. 83 (2004) 121–128.
[58] X. Xiao, S. Xiong, B. Li, Y. Geng, S. Yang, Role of $WO_3$ in NO reduction with $NH_3$ over $V_2O_5$-$WO_3$/$TiO_2$: a new insight from the kinetic study, Catal. Lett. 146 (2016) 2242–2251, https://doi.org/10.1007/s10562-016-1852-0.
[59] G.J. Dong, Y. Bai, Y.F. Zhang, Y. Zhao, Effect of the $V^{4+(3+)}/V^{5+}$ ratio on the denitration activity for $V_2O_5$-$WO_3$/$TiO_2$ catalysts, New J. Chem. 39 (2015) 3588–3596, https://doi.org/10.1039/c5nj00015g.
[60] J. Mendialdua, R. Casanova, Y. Barbaux, XPS studies of $V_2O_5$, $V_6O_{13}$, $VO_2$ and $V_2O_3$, J. Electron Spectrosc. Relat. Phenom. 71 (1995) 249–261, https://doi.org/10.1016/0368-2048(94)02291-7.
[61] G. Silversmit, D. Depla, H. Poelman, G.B. Marin, R. De Gryse, Determination of the V2p XPS binding energies for different vanadium oxidation states ($V^{5+}$ to $V^{0+}$), J. Electron Spectrosc. Relat. Phenom. 135 (2004) 167–175, https://doi.org/10.1016/j.elspec.2004.03.004.
[62] B. Rhimi, M. Mhamdi, A. Ghorbel, V.N. Kalevaru, A. Martin, M. Perez-Cadenas, A. Guerrero-Ruiz, Ammoxidation of ethylene to acetonitrile over vanadium and molybdenum supported zeolite catalysts prepared by solid-state ion exchange, J. Mol. Catal. A Chem. 416 (2016) 127–139, https://doi.org/10.1016/j.molcata.2016.02.028.
[63] Y. Suchorski, L. Rihko-Struckmann, F. Klose, Y. Ye, M. Alandjiyska, K. Sundmacher, H. Weiss, Evolution of oxidation states in vanadium-based catalysts under conventional XPS conditions, Appl. Surf. Sci. 249 (2005) 231–237, https://doi.org/10.1016/j.apsusc.2004.11.083.
[64] E. Kokkonen, F.L. Da Silva, M.H. Mikkela, N. Johansson, S.W. Huang, J.M. Lee, M. Andersson, A. Bartalesi, B.N. Reinecke, K. Handrup, H. Tarawneh, R. Sankari, J. Knudsen, J. Schnadt, C. Sathe, S. Urpelainen, Upgrade of the SPECIES beamline at the MAX IV Laboratory, J. Synchrotron Radiat. 28 (2021) 588–601, https://doi.org/10.1107/S1600577521000564.
[65] E.A. Redekop, N. Johansson, E. Kokkonen, S. Urpelainen, F. Lopes Da Silva, M. Kaipio, H.E. Nieminen, F. Rehman, V. Miikkulainen, M. Ritala, U. Olsbye, Synchronizing gas injections and time-resolved data acquisition for perturbation-enhanced APXPS experiments, Rev. Sci. Instrum. 92 (2021) 1–25, https://doi.org/10.1063/5.0039957.
[66] M.C. Biesinger, L.W.M. Lau, A.R. Gerson, R.S.C. Smart, Resolving surface chemical states in XPS analysis of first row transition metals, oxides and hydroxides: Sc, Ti, V, Cu and Zn, Appl. Surf. Sci. 257 (2010) 887–898, https://doi.org/10.1016/j.apsusc.2010.07.086.
[67] M.C. Biesinger, B.P. Payne, A.P. Grosvenor, L.W.M. Lau, A.R. Gerson, R.S.C. Smart, Resolving surface chemical states in XPS analysis of first row transition metals, oxides and hydroxides: Cr, Mn, Fe, Co and Ni, Appl. Surf. Sci. 257 (2011) 2717–2730, https://doi.org/10.1016/j.apsusc.2010.10.051.
[68] M. Tangirala, K. Zhang, D. Nminibapiel, V. Pallem, C. Dussarrat, W. Cao, T. N. Adam, C.S. Johnson, H.E. Elsayed-Ali, H. Baumgart, Physical analysis of $VO_2$ films grown by atomic layer deposition and RF magnetron sputtering, ECS J. Solid State Sci. Technol. 3 (2014) N89–N94, https://doi.org/10.1149/2.006406jss.
[69] K.H. Chang, C.C. Hu, $H_2V_3O_8$ single-crystal nanobelts: hydrothermal preparation and formation mechanism, Acta Mater. 55 (2007) 6192–6197, https://doi.org/10.1016/j.actamat.2007.07.018.
[70] K.D. Moulder, J.F., Stickle, W.F., Sobol, P.E. and Bomben, Handbook of X-Ray Photoelectron Spectroscopy, Perkin-Elmer Corporation, Eden Prairie, 1992.
[71] A.Y. Stakheev, E.S. Shpiro, J. Apijok, XPS and XAES study of $TiO_2$-$SiO_2$ mixed oxide system, J. Phys. Chem. 97 (1993) 5668–5672, https://doi.org/10.1021/j100123a034.
[72] S. Albonetti, S. Blasioli, A. Bruno, J.E. Mengou, F. Trifirò, Effect of silica on the catalytic destruction of chlorinated organics over V2O5/TiO2 catalysts, Appl. Catal. B Environ. 64 (2006) 1–8, https://doi.org/10.1016/j.apcatb.2005.10.017.
[73] N.E. Quaranta, J. Soria, V. Cortés Corberán, J.L.G. Fierro, Selective oxidation of ethanol to acetaldehyde on $V_2O_5$/$TiO_2$/$SiO_2$ catalysts: Effect of $TiO_2$-coating of the silica support, J. Catal. 171 (1997) 1–13, https://doi.org/10.1006/jcat.1997.1760.
[74] D.C.M. Dutoit, M. Schneider, R. Hutter, A. Baiker, Titania-silica mixed oxides: IV. Influence of Ti content and aging on structural and catalytic properties of aerogels, J. Catal. 161 (1996) 651–658, https://doi.org/10.1006/jcat.1996.0227.
[75] N. Seriani, C. Pinilla, S. Scandolo, Titania–silica mixed oxides investigated with density functional theory and molecular dynamics simulations, Phys. Status Solidi Basic Res. 254 (2017), https://doi.org/10.1002/pssb.201600510.
[76] I.E. Wachs, G. Deo, B.M. Weckhuysen, A. Andreini, M.A. Vuurman, M. de Boer, M. D. Amiridis, Selective catalytic reduction of NO with $NH_3$ over supported vanadia catalysts, J. Catal. 161 (1996) 211–221, https://doi.org/10.1006/jcat.1996.0179.
[77] G. Busca, A.S. Elmi, P. Forzatti, Mechanism of selective methanol oxidation over vanadium oxide-titanium oxide catalysts: a FT-IR and flow reactor study, J. Phys. Chem. 91 (1987) 5263–5269, https://doi.org/10.1021/j100304a026.
[78] I. Baldychev, J.M. Vohs, R.J. Gorte, The effect of support on redox properties and methanol-oxidation activity of vanadia catalysts, Appl. Catal. A Gen. 391 (2011) 86–91, https://doi.org/10.1016/j.apcata.2010.05.051.
[79] J. Döbler, M. Pritzsche, J. Sauer, Oxidation of methanol to formaldehyde on supported vanadium oxide catalysts compared to gas phase molecules, J. Am. Chem. Soc. 127 (2005) 10861–10868, https://doi.org/10.1021/ja051720e.
[80] S. Ojala, T. Laitinen, S. Leneuf de Neufville, M. Honkanen, M. Vippola, M. Huuhtanen, R.L. Keiski, Vanadia–zirconia and vanadia–hafnia catalysts for utilization of volatile organic compound emissions, Materials 14 (2021) 1–19, https://doi.org/10.3390/ma14185265.
[81] A.A. Ismail, I.A. Ibrahim, M.S. Ahmed, R.M. Mohamed, H. El-Shall, Sol-gel synthesis of titania-silica photocatalyst for cyanide photodegradation, J. Photochem. Photobiol. A Chem. 163 (2004) 445–451, https://doi.org/10.1016/j.jphotochem.2004.01.017.
[82] M. Ai, The relationship between the oxidation activity and the acid-base properties of $Fe_2O_3$-based mixed oxides. I. The $Fe_2O_3$-$V_2O_5$ and $Fe_2O_3$-$MoO_3$ systems, J. Catal. 52 (1978) 16–24, https://doi.org/10.1016/0021-9517(78)90118-5.
[83] S. Damyanova, M.L. Cubeiro, J.L.G. Fierro, Acid-redox properties of titania-supported 12-molybdophosphates for methanol oxidation, J. Mol. Catal. A Chem. 142 (1999) 85–100, https://doi.org/10.1016/S1381-1169(98)00279-9.